Appendix FF Discharge Dispersion Modelling Assessment

Discharge Dispersion Modelling

Iron Sand Mining Operations

Report prepared for Taharoa Ironsands Limited

June 2025

MetOcean SOLUTIONS

Document History

Versions

Version	Revision Date	Summary	Reviewed by
0.1	14/03/2025	Draft for internal review	Cussioli
0.2	14/03/2025	Draft for Client review	Berthot/Cussioli

Distribution

Version	Date	Distribution
1.0	01/07/2025	Taharoa Ironsands Limited

Document ID: P0564

Authors

Cussioli M., Berthot A

This report has been prepared for Taharoa Ironsands Limited in respect of its application for all approvals under the Fast-track Approvals Act 2024 for the Central and Southern Blocks of the Taharoa Ironsand Mine. The Panel appointed to consider the application for the Central and Southern Blocks Mining Project may rely on this report for the purpose of making its decision under the Fast-track Approvals Act 2024.

This report has been prepared in accordance with the Environment Court's Code of Conduct for expert witnesses, contained in the Environment Court's Practice Note 2023. The authors of this report agree to comply with the Code of Conduct, and confirm that unless otherwise stated, the issues addressed in this report are within the area of expertise of the authors. No material facts have been omitted that might alter or detracted from the opinions expressed in this report.

Contents

List of Figures

List of Tables

1.Introduction

Taharoa Ironsands Limited is preparing an application under the Fast-track Approvals Act to Waikato Regional Council to undertake iron sand mining operations near Taharoa (Application No APP142035), located on the west coast of the North Island of New Zealand approximately 20 km south of Kawhia Harbour (Figure 1.1).

The iron sand is mined by either a Dry Mining Unit (DMU) or a cutter suction dredge within a created pond. The mined sand is mixed with water and pumped to the separation plant. After passing through a magnetic separator, the concentrated iron sand is pumped as a slurry out through submarine pipes connected to a single point mooring buoy 3.5 km from the shore (Figure 1.2). The buoy location is exposed and subject to storms and high waves. Loading iron sand to a bulk carrier ship at the buoy is restricted by weather and swell conditions.

Before loading, the ship is prepared to receive the slurry by pumping fresh water into the holds to provide protection from damaging the hold floor. The percentage of iron sand concentrate is then increased by discharging the excess fresh water, which may contain fine particles in suspension (Figure 1.3). The discharge also includes the water used to fluidise the ironsand to allow pumping to the ship.

The consent for the ship loading operation is for a release of 75,000 m^3 of de-watering fluid (including freshwater and fine sediment) per day, to a maximum of 7,500,000 m^3 per year.

MetOcean Solutions has previously undertaken a plume dispersion and deposition modelling (MetOcean Solutions, 2022) which was based on the release of a total 3,600,000 m^3 of de-watering fluid per year. The modelling considered the release of 150,000 m^3 over 48 hours (75,000 m^3 per day) every 15 days, for representative three-month periods over summer and winter.

Taharoa Ironsands has requested that the modelling is updated to simulate the total de-watering volume proposed to be discharged each year (7,500,000 m^3), as opposed to a representative sample.

To understand the transport of sediment from the discharge, sediment plume and deposition, a comprehensive consideration of coastal process is required which include an assessment of plume dynamics and dispersal (duration/extent), settling conditions, weather events and the other effects that may persist and propagate resuspension of discharged material.

For this purpose, we used a calibrated and validated Delft3D model to simulate scenarios of sediment release representing the discharge of water during ship loading for two contrasting periods (summer and winter). Results are presented as maps of percentile of sediment concentration and potential areas of sediment deposition.

The report is structured as follows: the methods applied in this study are presented in Section 2, model validation and results are described in Section 3. A summary of findings is provided in Section 4, and the references cited are listed in Section 5.

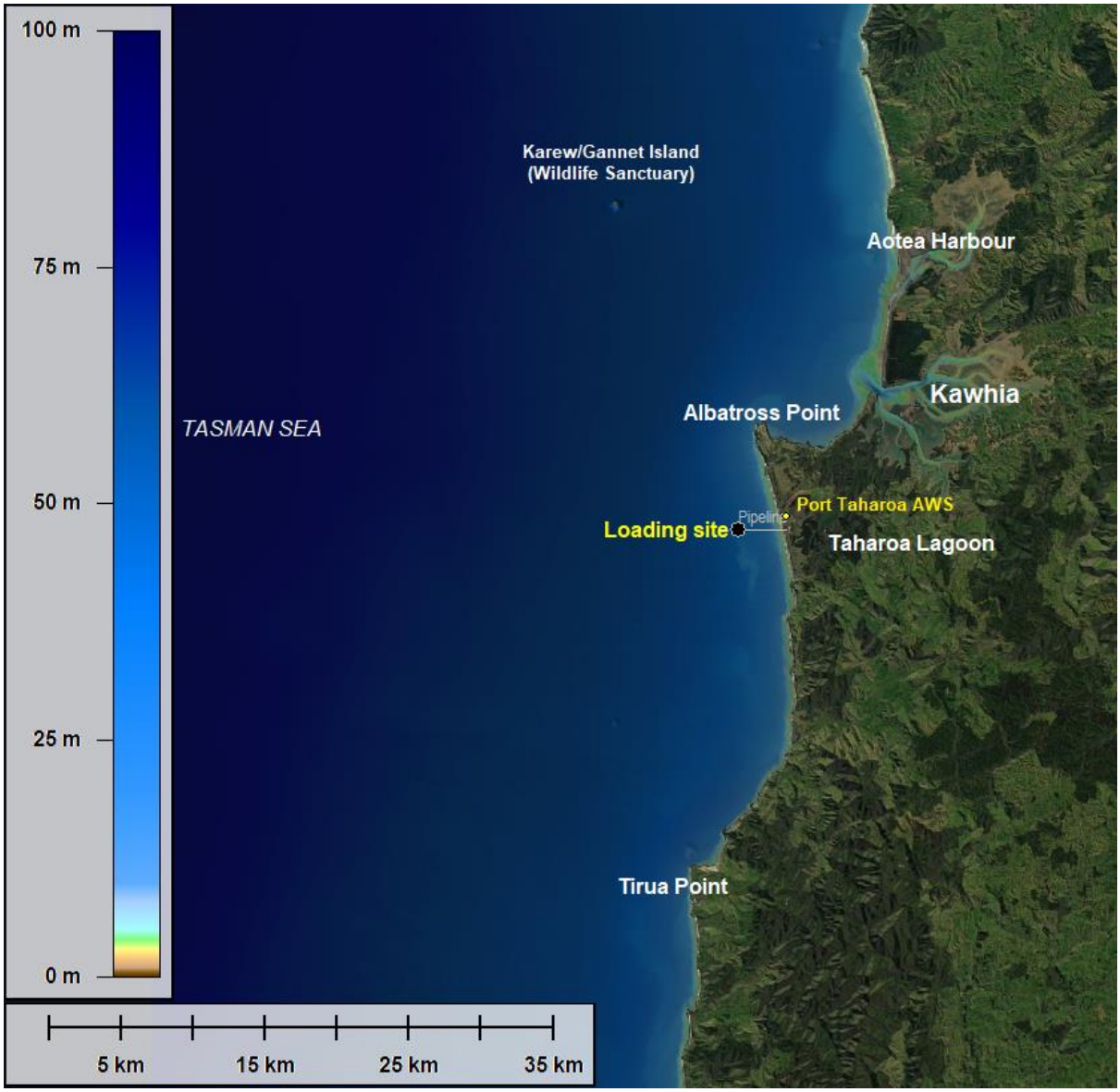

Figure 1.1 Taharoa Terminal and surrounding area, with interpolated bathymetry data. The submerged pipeline leads to the offshore mooring buoy (Loading site).

Figure 1.2 Ship loading at Taharoa terminal. Source: Engineering NZ[1].

Figure 1.3 Plume of water and fine particles discharged during ship loading operation. Source: personal communication with Jared Pettersson (Enviser).

[1] *https://www.engineeringnz.org/programmes/heritage/heritage-records/taharoa-ironsand-mining-and-ship-loading/ (Image courtesy of M. Lye, New Zealand Steel Limited).*

1.1 Background

At the central West Coast of the North Island, sediment transport is mainly northwards along the continental shelf (Figure 1.4 – top panel) related to prevailing weather patterns and direction of main circulation. Fine sediment is generally transported to the coast by rivers and tends to flocculate and settle nearshore. Nearshore areas that are exposed to waves are likely to experience sediment resuspension by waves, making some of the sediment available to be transported by the mean circulation, tides, and storm-driven components (Carter & Heath, 1975).

A more recent study carried out by Hunt and Jones (2020) looked at plume fate using idealised model simulations and satellite images. In their study, they show the influence of wind speed on plume fate patterns, e.g., plumes from Aotea and Kawhia are directed southwards under light (<5 $m.s^{-1}$ SW or <10 $m.s^{-1}$ E) winds and northwards under stronger (>5 $m.s^{-1}$ SW) winds. The modelling did not include wave forcing and did not consider particle settling, however, the authors discuss the high energy wave conditions throughout the study area are likely to provide an important control on the patterns of deposition. Wave orbital velocities would mobilise fine sediment that could be transported offshore or transported into the estuaries during flood tide.

Available information on sediment concentration around the area is scarce. In terms of sediment yield, Hicks et al. (2011) estimated that the West Coast of the North Island potentially contribute 3.96-4.12 $Mt.y^{-1}$ of river suspended sediment, about 0.5% of the total fine sediment delivered to New Zealand's entire coastal regions (Figure 1.4 – bottom panel).

Information on background suspended sediment concentration is available for an area located approximately 200-300 km south of Taharoa, at the South Taranaki Bight (MacDonald et al., 2012). Water quality investigations showed that near-surface background suspended sediment concentration for this area is typically less than 10 mg.l-1 most of the time, with maximum concentrations of 25 mg.l-1. Peaks of concentration usually occurred at times of large waves. It should be noted that the South Taranaki Bight area has different coastline orientation compared to the study site, the proximity to the Cook Strait, and different river sediment yield (12.1 Mt.y-1 for Southwest Coast - Hicks et al. 2011).

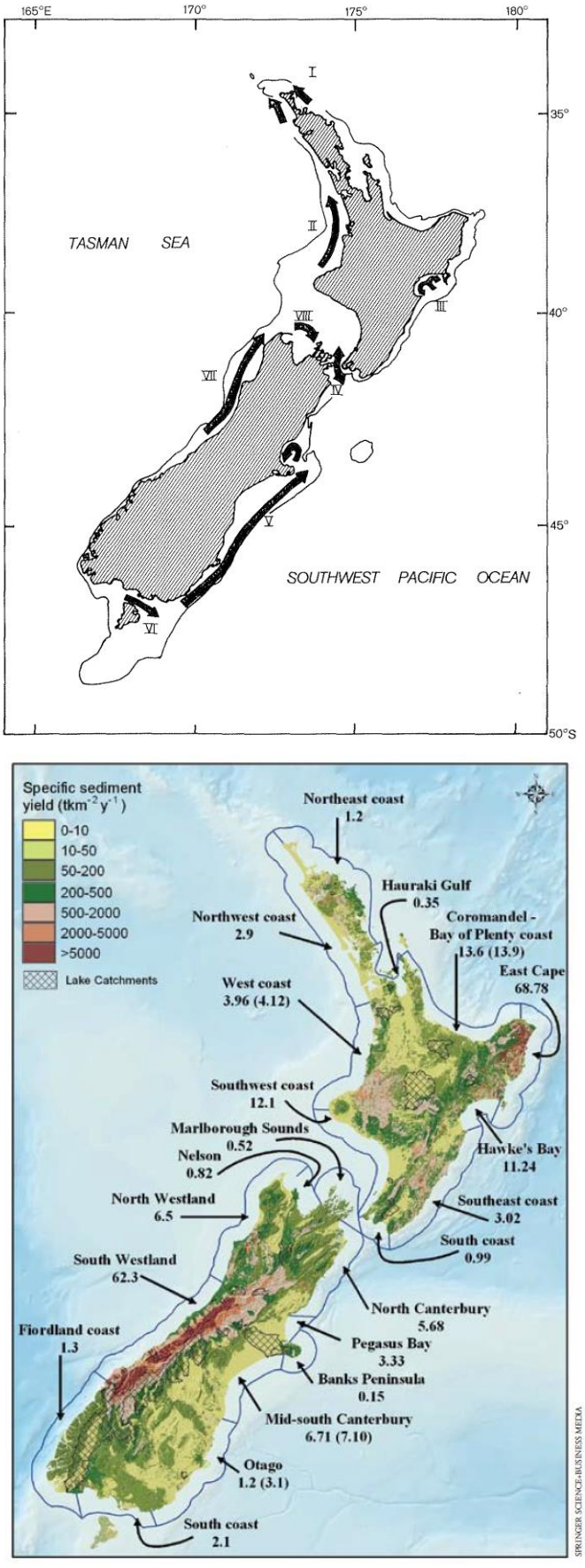

Figure 1.4 Directions of sediment transport over the continental shelf from Carter and Heath (1975) (top panel) and sediment yields to coast (Mt/y) totalled by region from Hicks et al. (2011) (bottom panel).

2.Methods

2.1 Bathymetry

Bathymetry data was amalgamated in a GIS environment from a variety of sources including LiDAR data in the shallow intertidal regions, local single-beam surveys in the shallow harbour/estuary entrances, electronic navigation chart data and digitised fare sheets (Figure 2.1 and Figure 2.2).

Data was sourced in a variety of datums and projections, all converted to NZTM2000 and Mean Sea Level (MSL), which is required within the modelling space (Figure 2.3). Based on an analysis by NIWA at Kawhia tide gauge between 2008 and 2014, MSL is 0.13 m above MVD (Moturiki vertical datum). Chart Datum (CD) to msl offsets varied between 1.83 and 2.369m depending on the fare sheet.

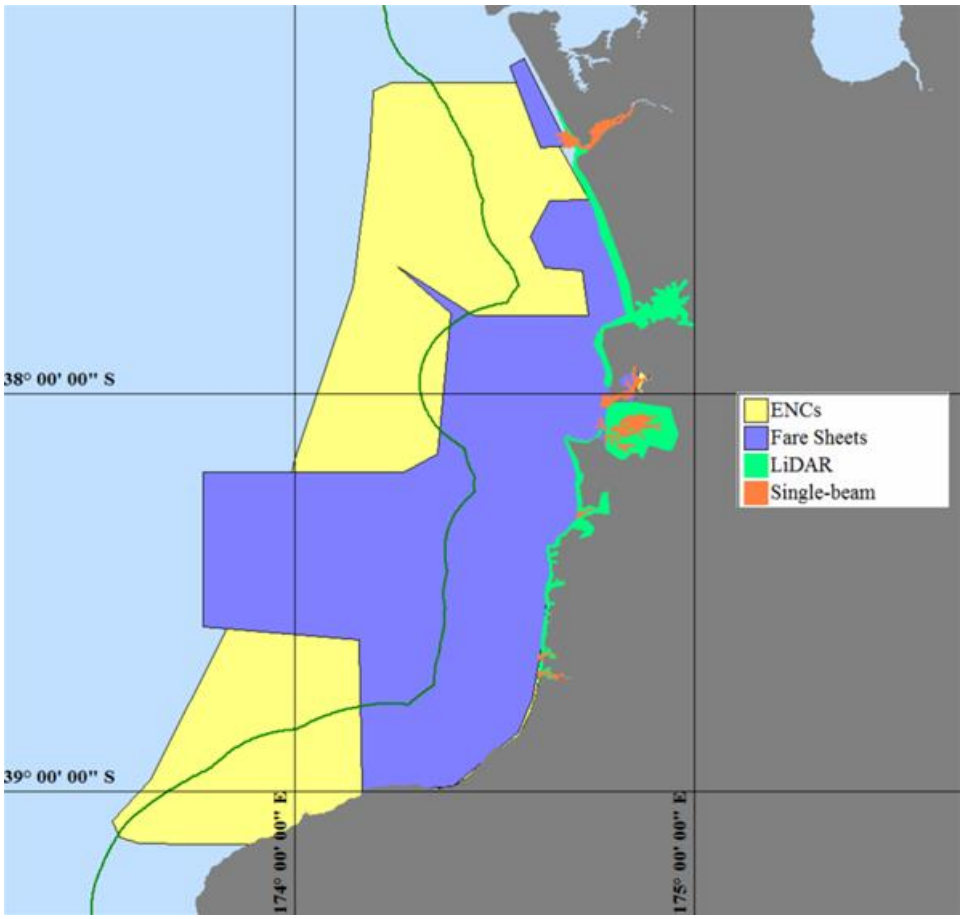

Figure 2.1 Sources and location of raw bathymetry data. The 12 nautical mile territorial sea limit is indicated as a green line.

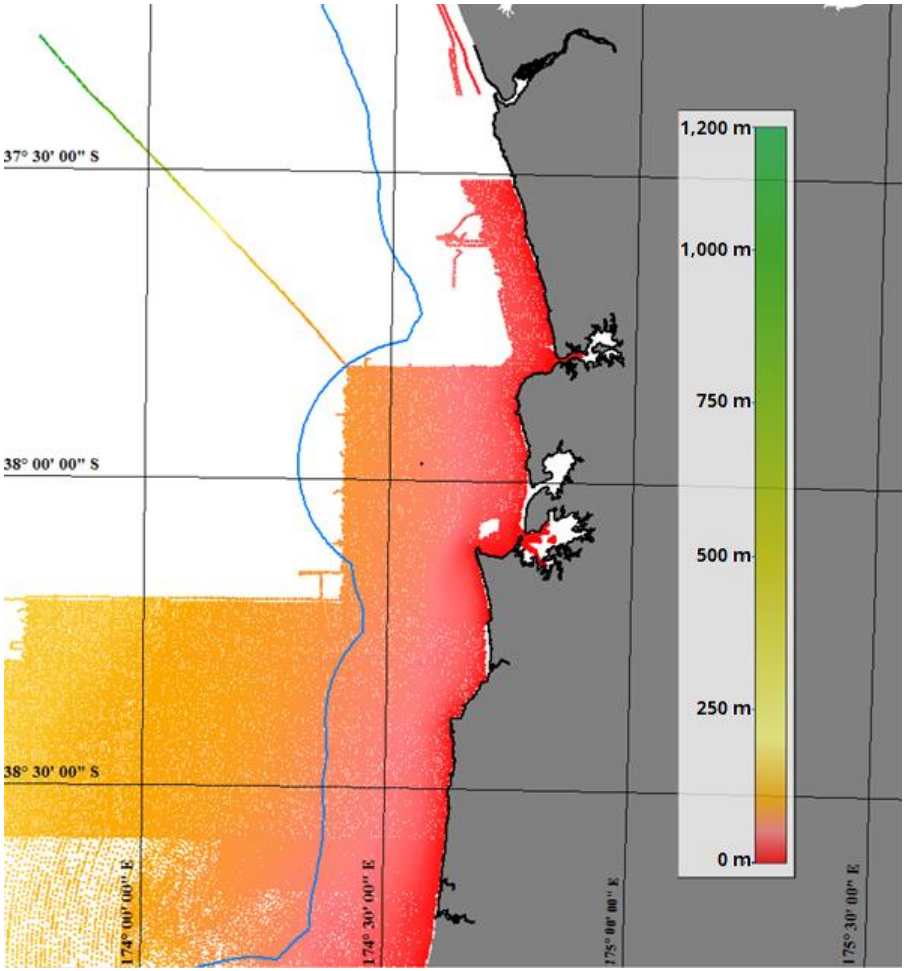

Figure 2.2 Fare Sheets data coverage.

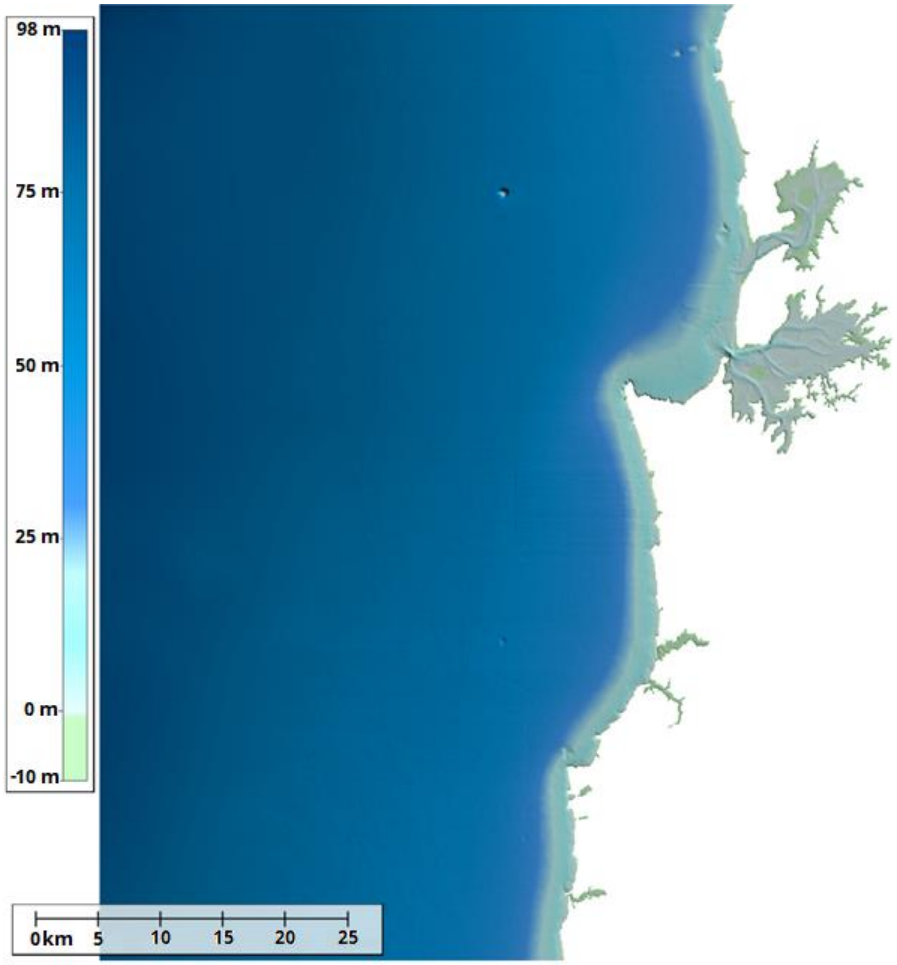

Figure 2.3 50m-resolution Taharoa grid (relative to mean sea level).

2.2 Sediment dispersal modelling

2.2.1 Model description

The modelling system Delft3D (Deltares, 2018) was used in this study. The software is based on interlinking three separate components (Delft3D – WAVE, Delft3D – FLOW and Delft3D – MOR) that together simulate multi-dimensional hydrodynamic flows, waves and sediment transport. The three components are fully coupled.

Delft3D has been specifically developed to simulate the dynamics of complex coastal regions controlled by a wide range of physical and morphological processes. Delft3D has been successfully applied worldwide to a wide range of coastal studies, including, within the New Zealand context, Port Otago (Weppe et al., 2015), Tauranga Harbour (Ramli et al., 2015) and Rees River (Williams et al., 2016).

The following subsections give a brief description of the different Delft3D modules used in this study.

2.2.1.1 Delft3D - WAVE

The third-generation SWAN model (Simulating WAves Nearshore) is used in the wave module (Booij et al., 1999; Ris et al., 1999). SWAN computes the evolution of random, short-crested waves in coastal regions with deep, intermediate and shallow water depths. Wave forces computed by the wave module on the basis of the radiation shear stress gradients can be used as a driving force to compute the wave-induced currents and set-up in the flow module.

2.2.1.2 Delft3D - FLOW

The hydrodynamic module is a 2D or 3D hydrodynamic model which calculates non-steady flows and transport processes. Delft3D – FLOW solves the Navier – Stokes equations on a staggered model grid for an incompressible fluid under the shallow water and Boussinesq assumptions. The system solves the horizontal equations of motion, the continuity equation, the transport equations for conservative constituents and a turbulence closure scheme.

2.2.1.3 Delft3D – MOR

The sediment transport module integrates the effects of waves and currents. At each computational time step the model computes both bedload and suspended-load sediment transport components within the model domain. The bed level is then updated as a result of sediment sink and sources terms and transport gradients. The model is able to simulate the sediment dynamics associated with both non-cohesive (sandy) and cohesive (silt/mud) sediments.

2.2.2 Model domain

The model domain covers an area extending approximately 35 km north and south of Taharoa terminal (Figure 2.4), with high resolution (100 m) at the discharge site and within harbours/estuaries and approximately 200-400 m resolution elsewhere for model efficiency. Bathymetry data was interpolated on the model grid and set at 0 m at mean sea level (MSL, Figure 2.5).

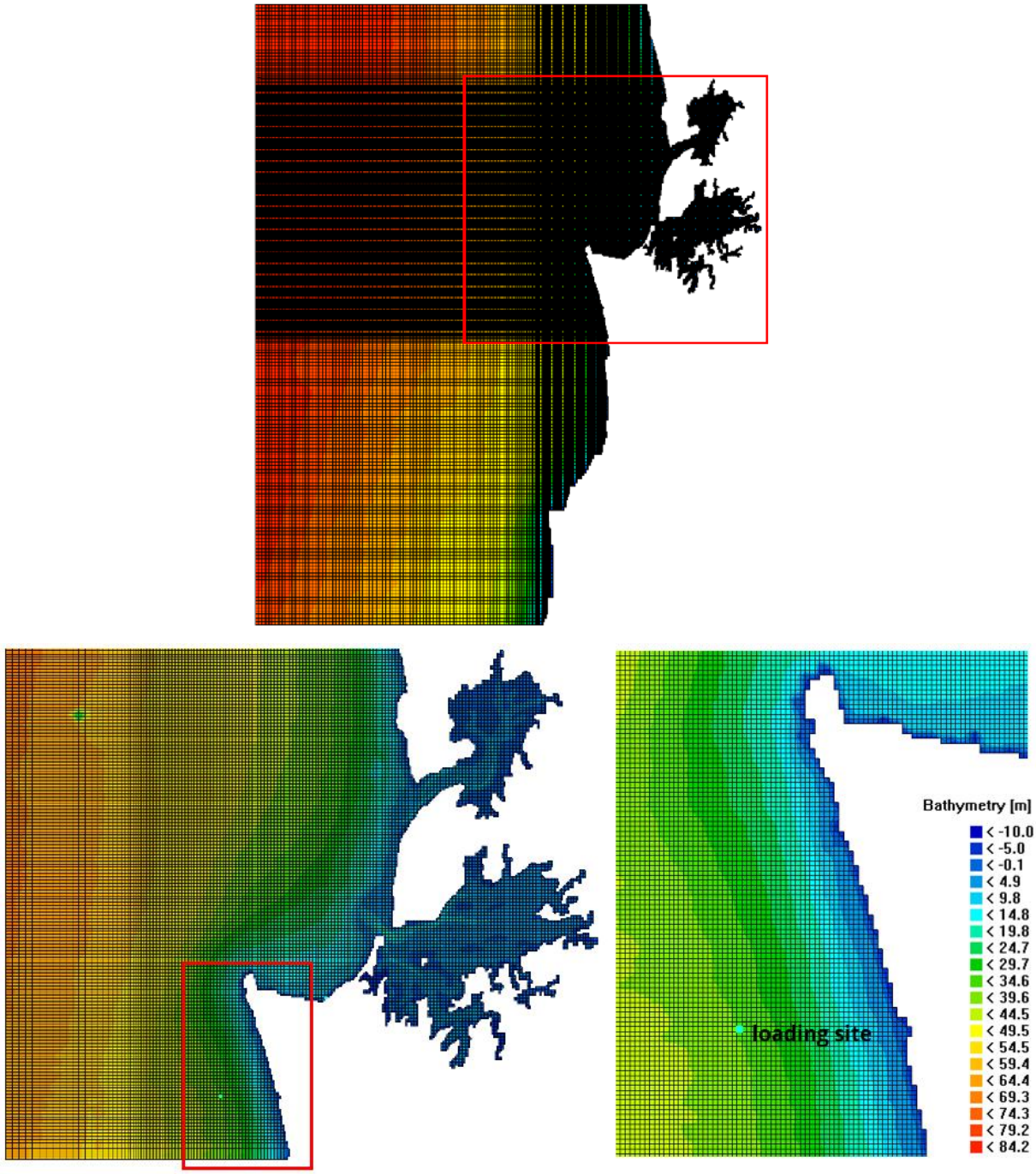

Figure 2.4 Model domain full grid extension (top) and detailed grid at the ship loading site (right).

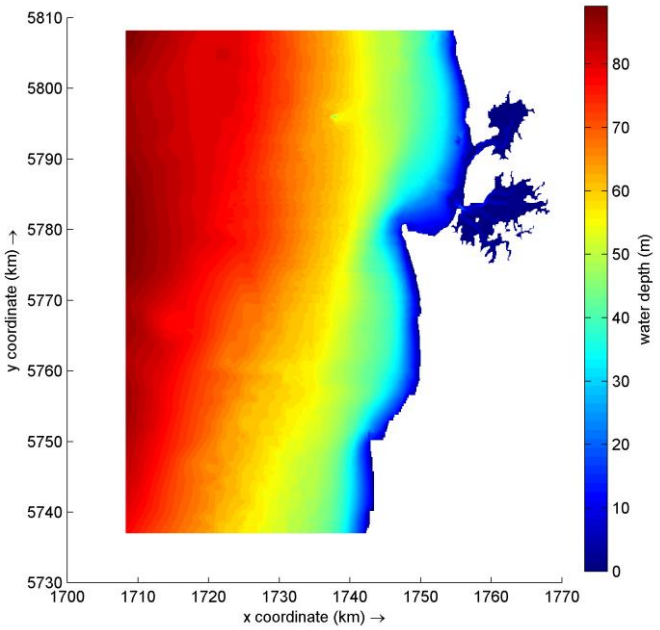

Figure 2.5 Model bathymetry (MSL).

2.2.3 Model forcing

The modelling of the sediment dispersion aimed at capturing a range of possible hydrodynamic forcing expected near the site in order to provide a robust picture of the likely dispersion and deposition patterns.

In this study, the modelling approach involved simulating two distinct periods (summer and winter) of 3-months each with a sediment discharge representing the release of the vessel hold water volume with fines sediment. The hydrodynamic and sediment model ran coupled with waves which are likely to maintain in suspension or resuspend sediment nearshore, thus having an important contribution on plume footprint.

2.2.3.1 Waves

The wave hindcast is available over a 41-year period (Jan 1979–Dec 2019) using the latest version of SWAN (Simulating WAves Nearshore). Full spectral boundaries to the parent 4-km SWAN domain of the North Island of New Zealand were prescribed from a global implementation of WAVEWATCH III (WW3) spectral wave model (Tolman, 1991) run at 0.5° resolution using the source term parameterisations of Ardhuin et al. (2010). A snapshot of model output for SWAN domain are shown in Figure 2.6.

The year of 2010 was carefully selected based on the offshore sea state corresponding to the closest values from the 23-year period (1994–2016) averaged conditions (Table 2.1). The period of 1994–2016 is based on the period of data available for the other model forcing (i.e., currents and wind).

Timeseries of wave hindcast parameters (Hs, Tp and Dpm) covering 3 months of winter (Jun-Jul-Aug 2010) and summer (Jan-Feb-Mar 2010) periods were extracted from MetOcean Solutions existing SWAN wave hindcast at representative sites at the north, west, and south Delft3D-WAVE boundaries (Figure 2.7 and Figure 2.8). The windroses show more energetic wave events in winter compared to summer months, and an increased predominance of SWW waves in winter for the north and west boundaries.

Bottom friction was modelled using the formulation of Collins (1972) and the default coefficient value was 0.015. Wave breaking was modelled using a constant critical wave height to water depth ratio of 0.73 with a proportionality coefficient for the rate of dissipation of 1. Wind was applied in the hydrodynamic module and coupled to the wave module. In these simulations, the wave conditions were updated every hour using the hydrodynamic field provided by the hydrodynamic module.

Table 2.1 Annual significant wave height statistics at approximate location of ship loading site (WGS84 Lat/Lon: -38.1751, 174.6672) and offshore (WGS84 Lat/Lon: -38.1751, 174.2336). This table shows the selected year of simulation (2010) with mean and 95th percentile Hs closest to the averaged values.

Year	Parameter Hs at Loading site		Parameter Hs at Offshore site	
	Mean (m)	95th percentile (m)	Mean (m)	95th percentile (m)
1994	2.08	3.61	2.63	4.68
1995	1.90	3.38	2.44	4.26
1996	1.83	3.44	2.38	4.36
1997	1.93	3.25	2.45	4.11
1998	1.96	3.29	2.54	4.20
1999	1.76	3.02	2.25	3.85
2000	1.84	3.10	2.36	3.93
2001	1.70	3.09	2.19	3.87
2002	1.95	3.59	2.49	4.61
2003	1.80	3.10	2.31	3.99
2004	1.99	3.57	2.55	4.52
2005	1.81	3.07	2.29	3.84
2006	2.06	3.49	2.58	4.32
2007	1.84	3.46	2.34	4.32
2008	1.94	3.56	2.50	4.53
2009	1.87	3.30	2.38	4.12
2010	**1.98**	**3.48**	**2.49**	**4.34**
2011	1.96	3.79	2.51	4.75
2012	1.97	3.44	2.51	4.41
2013	1.97	3.39	2.46	4.12
2014	2.09	3.69	2.65	4.55
2015	2.13	3.69	2.66	4.61
2016	2.14	4.03	2.69	5.06
Average	**1.93**	**3.43**	**2.46**	**4.33**

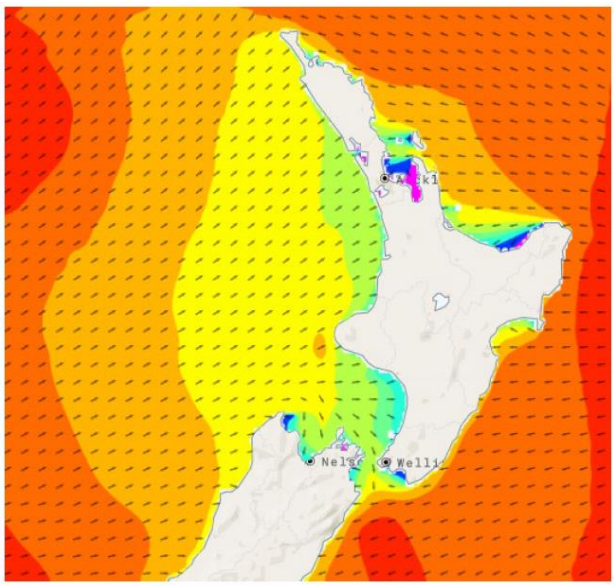

Figure 2.6 Snapshots of significant wave height from the NZN 4-km SWAN parent domain.

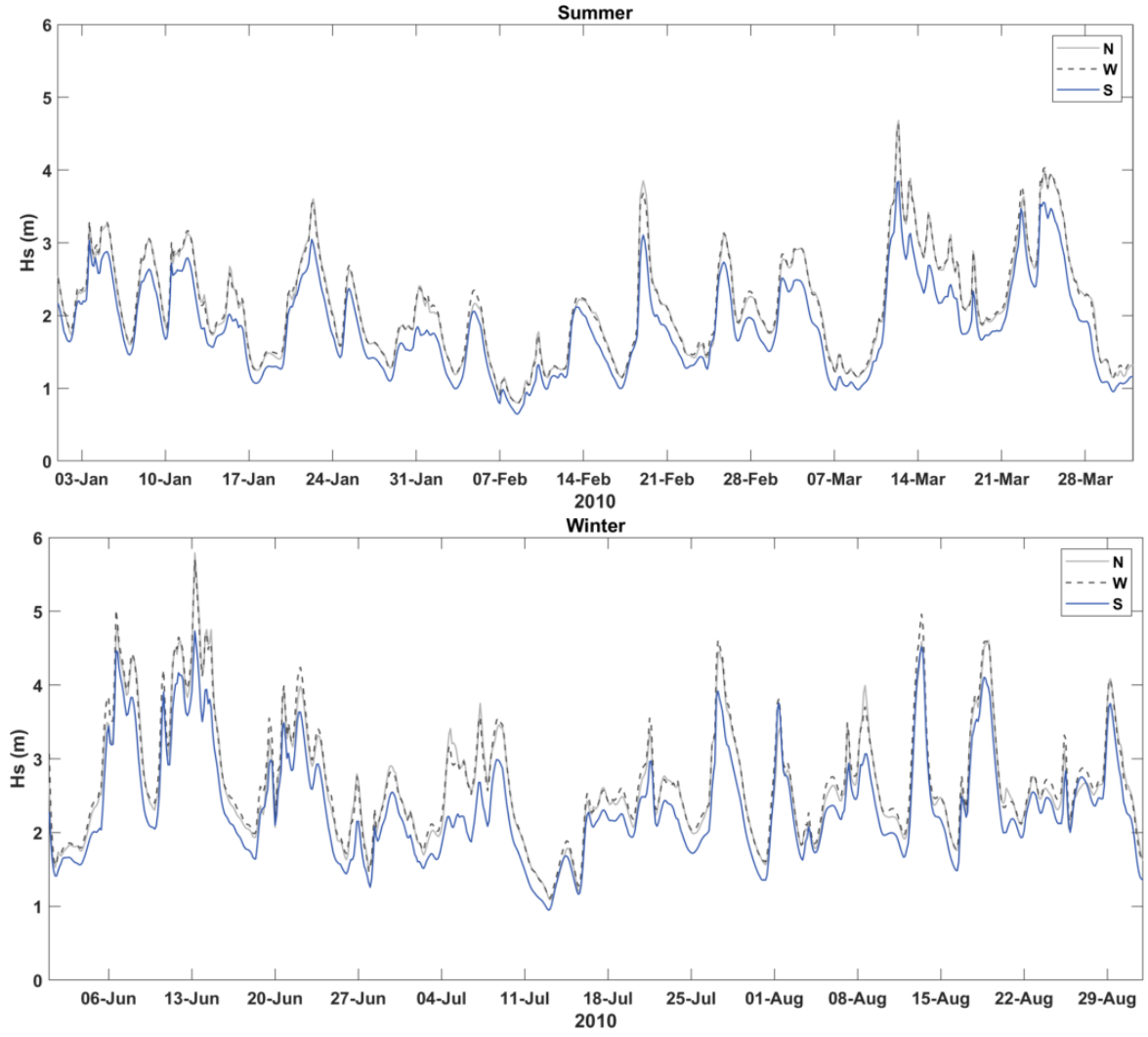

Figure 2.7 Significant wave height (Hs) from SWAN hindcast for summer (top) and winter (bottom) at the centre of the North (N), West (W), and South (S) boundaries.

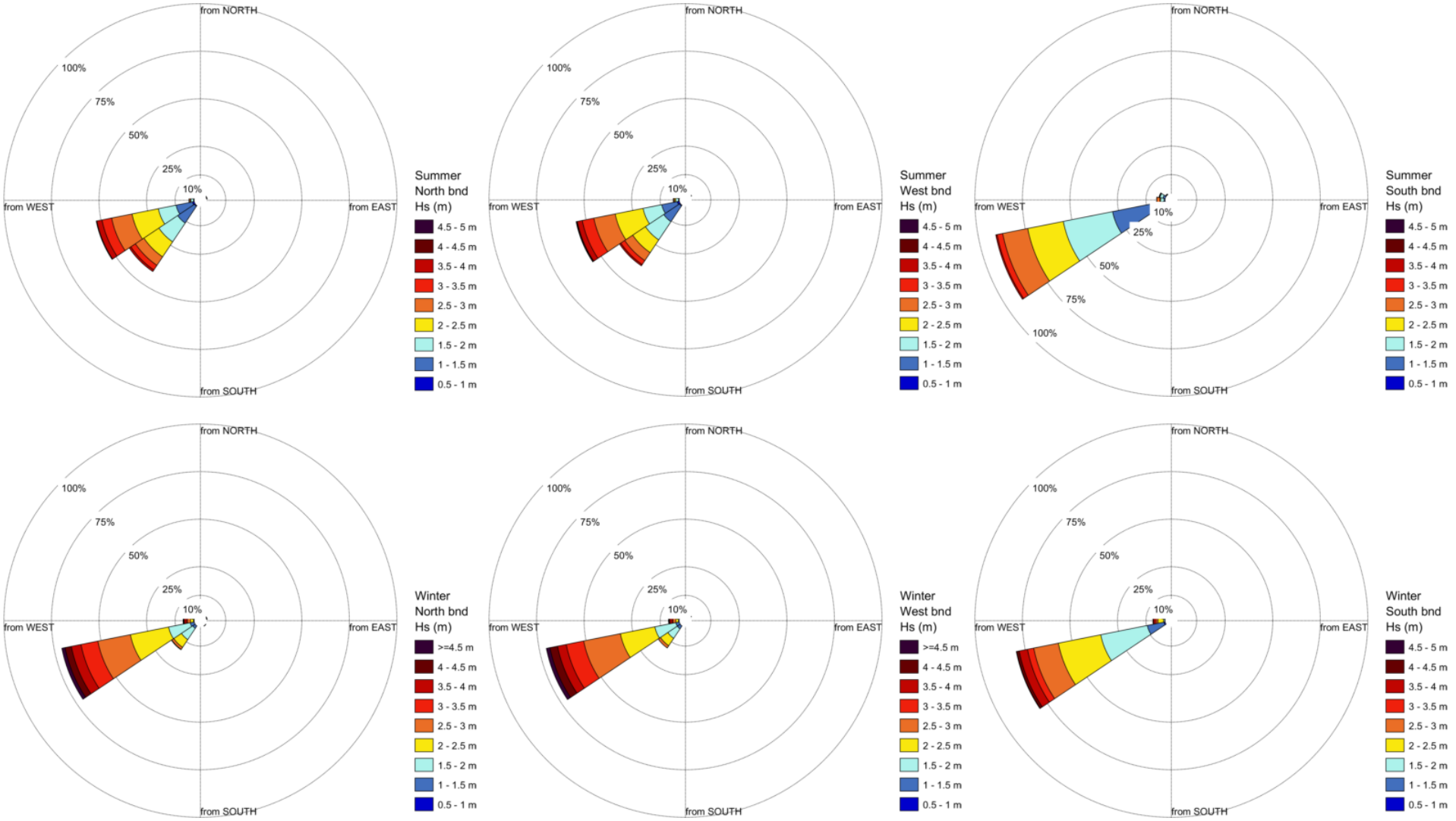

Figure 2.8 Wave hindcast (SWAN) for summer 2010 (top) and winter 2010 (bottom) at the centre of the North, West, and South boundaries (Bnd)

2.2.3.2 Hydrodynamics

The Delft3D-FLOW model was forced at the offshore boundaries with the latest high-resolution ROMS backbone model outputs which have been calibrated and validated against field data available around New Zealand.

The ROMS spatial resolution is approximately 5x5 km and include the whole New Zealand (Figure 2.9). A total of 40 vertical sigma layers were used in ROMS. The ROMS model was run in three-dimensional mode and was nested within the global GLORYS/Mercator reanalysis 12v1 (latest version from Nov 2018) at daily intervals and 8 km spatial resolution (Ferry et al., 2012). The atmospheric forcings were sourced from the CFSR reanalysis (Saha et al., 2010). Spectral tidal forcings were imposed at the ROMS domain boundaries by the Oregon State University Tidal Inverse Solution (OTIS), widely used to force regional and coastal domains in hydrodynamic models (Egbert & Erofeeva, 2002). A total of 11 tidal constituents were used.

Delft3D-FLOW ran in 3D with 7 layers in the vertical, representing 4%, 6%, 15%, 50%, 15%, 6%, and 4% of total depth, from surface to bottom, respectively. Thickness was reduced near the surface and bottom layers to resolve the logarithmic profile of the horizontal velocity components in the vertical.

Water levels and currents were prescribed as Riemann boundaries for several segments along the north, west, and south boundaries. The currents prescribed at the model boundaries (Figure 2.10) were extracted from depth averaged ROMS outputs and applied as 3D logarithmic vertical profiles in Delft3D-FLOW.

Bed shear stresses are computed using a standard quadratic friction law. The non-linear enhancement of the bed shear stress in presence of waves was taken into account by means of the wave-current interaction model of Fredsøe (1984). Turbulence effects are modelled using constant background horizontal and vertical eddy viscosity and eddy diffusivity coefficients. Horizontal background eddy viscosity and diffusivity are set to 1 $m^2.s^{-1}$ and 10 $m^2.s^{-1}$, respectively. A value of $10e^{-4}$ is used for the vertical background viscosity and diffusivity.

A time step of 6 seconds was used for the Delft3D-FLOW simulations, equivalent to maximum Courant numbers of less than 4. The Courant number is a numerical stability criterion that needs to be less than 10 in Delft3D-FLOW (Deltares, 2013).

Wind data from ERA5[2] reanalysis (Hersbach et al., 2018) was compared to measured data at the Port Taharoa AWS Station located at LAT/LON -38.166 /174.705 to verify the suitability of the reanalysis data for the region (Figure 2.11 and Figure 2.12). Reanalysis combines model data with observations from across the world into a globally complete and consistent dataset. ERA5 provides hourly data from 1979 to present.

The two datasets show good agreement, with ERA5 slightly underestimating the wind speed and increasing contribution of winds coming from WSW. The general directional pattern observed at the AWS, with winds mainly coming from W and SE sectors, is also represented in the reanalysis.

The near surface 3-month (summer and winter) wind timeseries to force model runs were extracted from the ERA5 reanalysis (Figure 2.13 and Figure 2.14).

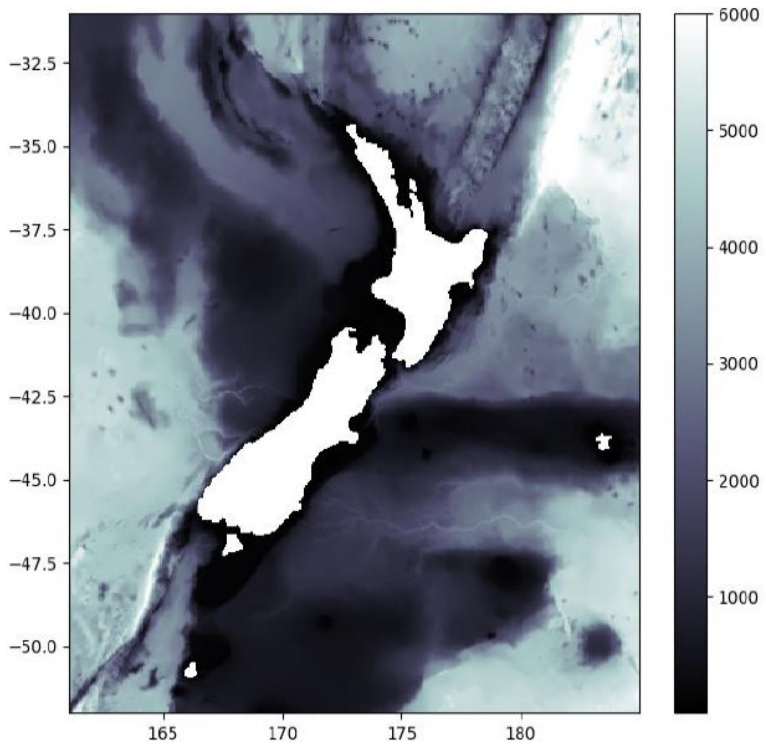

Figure 2.9 Bathymetry map showing the extents of the hydrodynamic regional ROMS domain at approximately 5 by 5 km resolution.

[22] https://confluence.ecmwf.int/display/CKB/The+family+of+ERA5+datasets

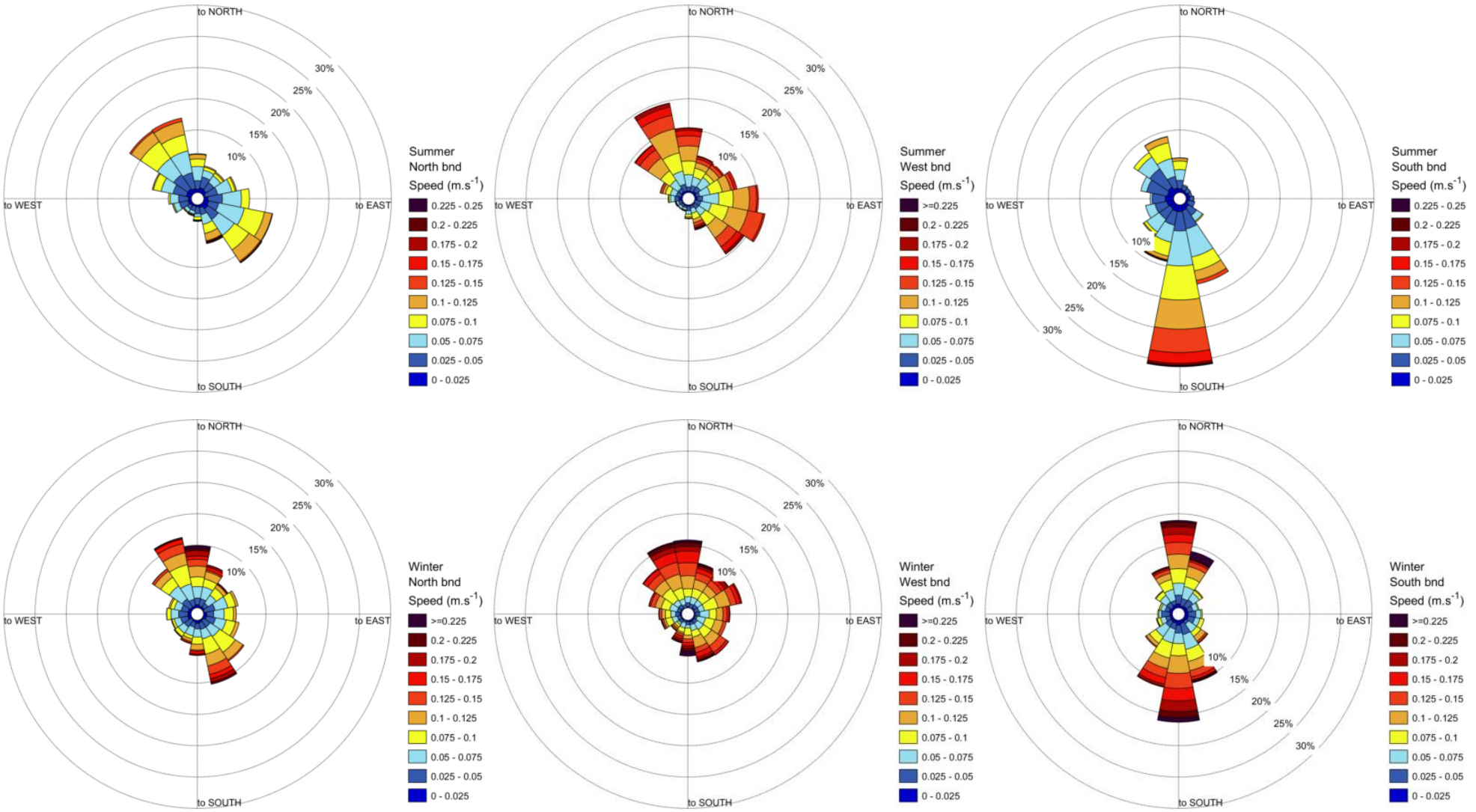

Figure 2.10 Current hindcast (ROMS) for summer 2010 (top) and winter 2010 (bottom) at the centre of the North, West, and South boundaries (Bnd)

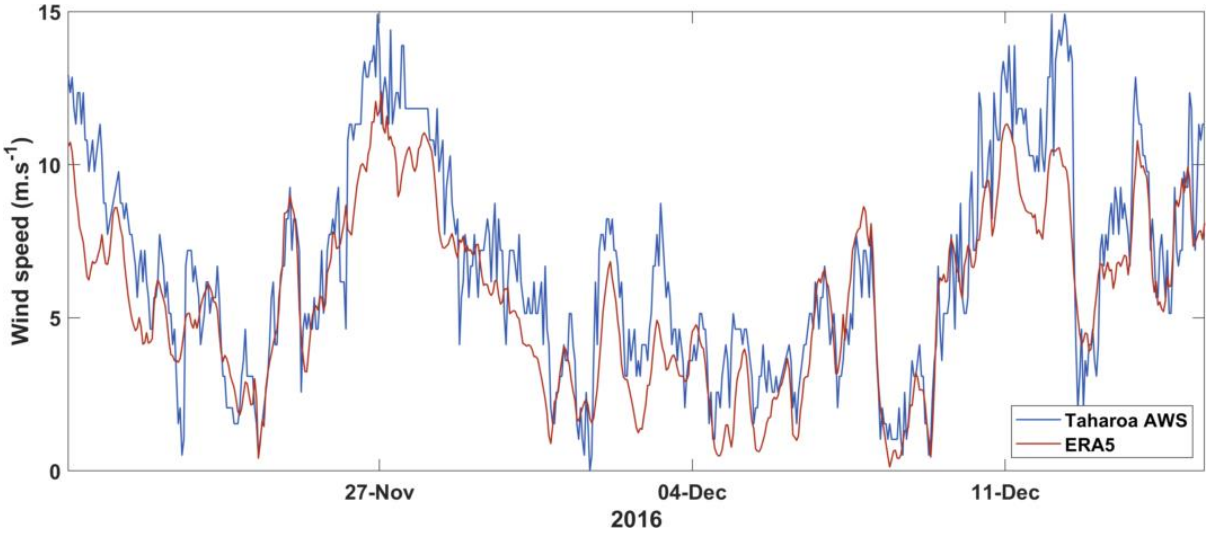

Figure 2.11 Comparison between wind speed measured at Taharoa AWS and extracted from ERA5 Reanalysis.

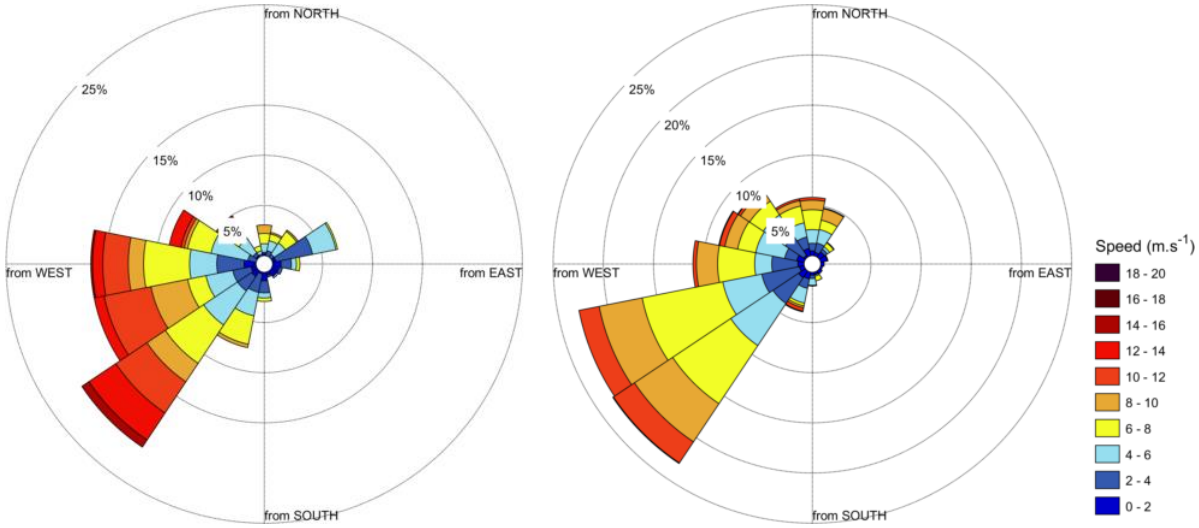

Figure 2.12 Windroses for measured data at Taharoa AWS (left) and extracted from ERA5 Reanalysis (right).

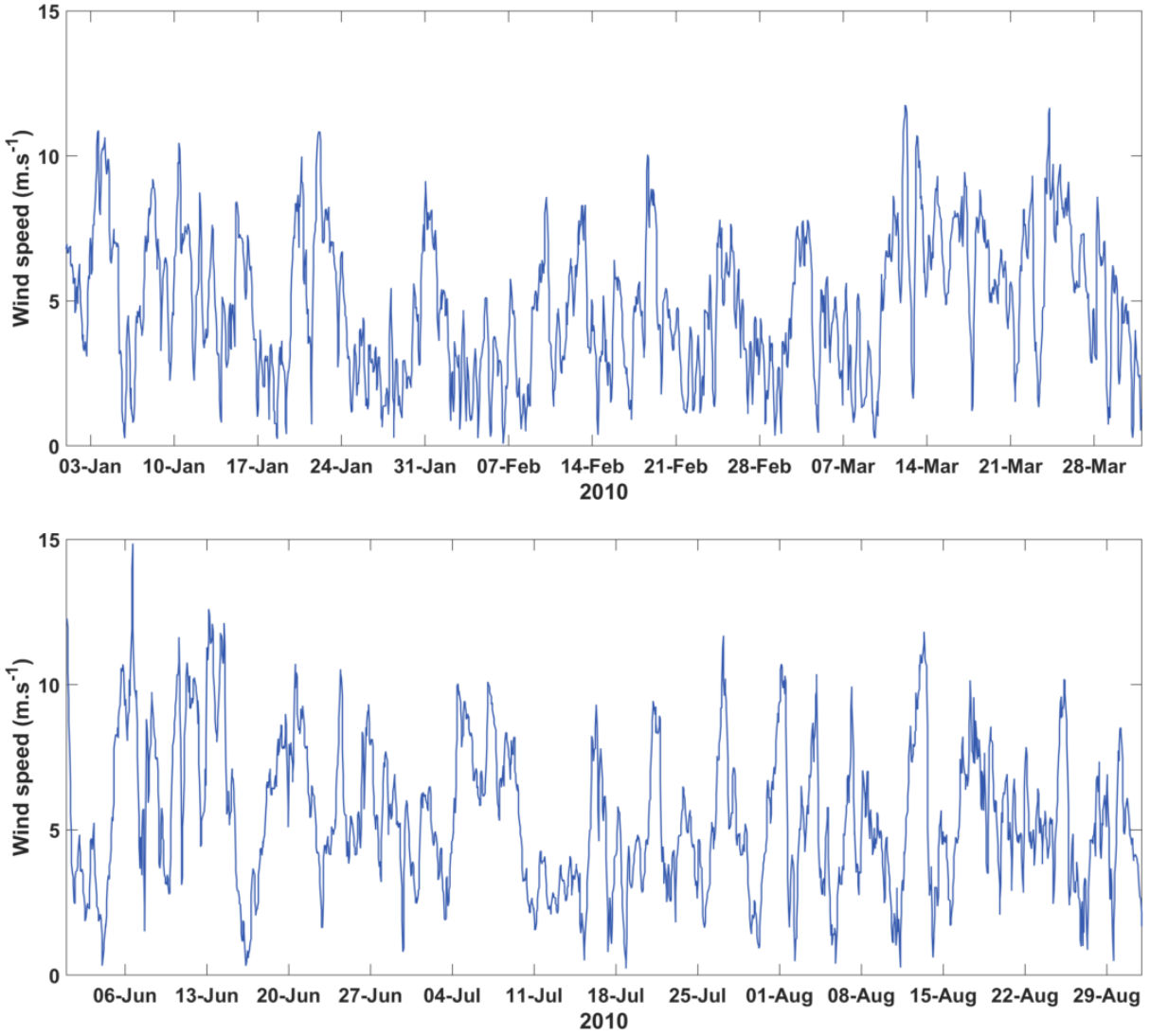

Figure 2.13 Wind speed (ERA5) for summer 2010 (top) and winter 2010 (bottom) used in the model simulations.

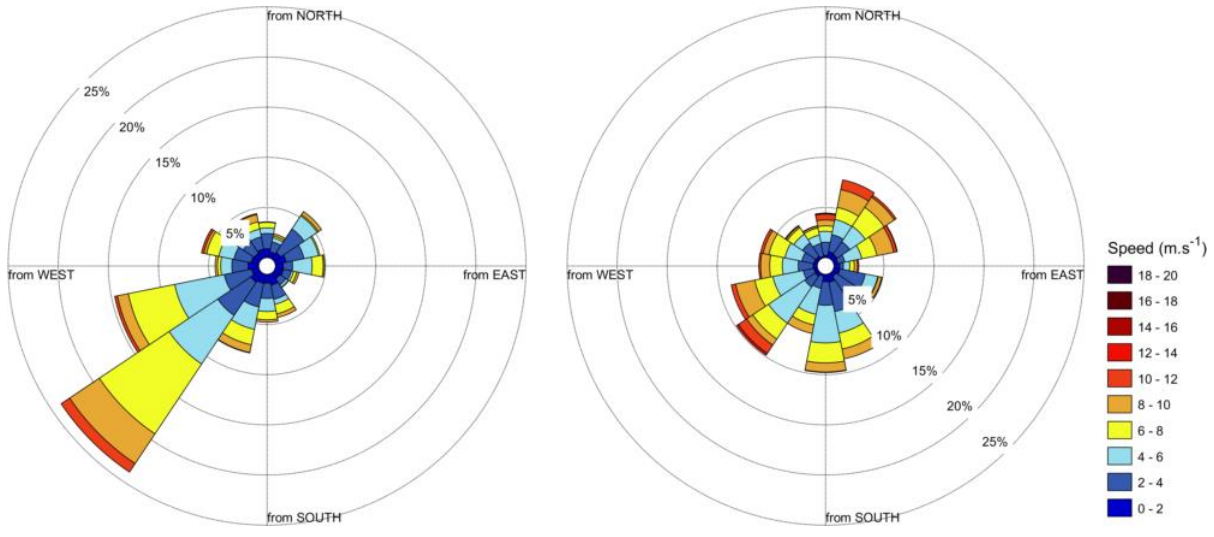

Figure 2.14 Windroses for summer (left) and winter (right) extracted from ERA5 and used in the model simulations.

2.2.3.3 Sediments

The present study considered one class of fine cohesive sediment in the discharge representative of a sediment size of 10 µm (average D50 in Table 2.2). Particle size analysis of samples taken in 2020 and 2021 have identified that most of the particles can be characterised as very fine to medium silt (4-31 µm) with only one sample of D50 in the clay range (<4 µm) (Table 2.2). We used a settling velocity of 0.02 $cm.s^{-1}$ to take in consideration the discharge of particles in seawater and therefore represent the relative increase in settling due to particle flocculation (when compared to settling in freshwater).

Analysis of samples taken from the ship loading water before discharge (i.e. within the ship) shows concentration of particles (TSS) is in average 1,082any $mg.l^{-1}$ (1.082 $kg.m^{-3}$) (Table 2.3).

Table 2.2 Particle size diameters D10, D50 and D90 of samples taken in 2020 and 2021. Analysis was carried out by Malvern Instruments Ltd using a laser diffraction particle size analyser and provided by Taharoa IronSands Ltd.

	SAMPLE	D10 (µm)	D50 (µm)	Dv90 (µm)
2020	TE34-1	5.87	15.00	38.10
	TE34-2	3.05	8.82	27.30
	TE34-3	4.92	13.60	144.00
	TP16-1	3.46	8.86	24.10
	TP16-2	6.13	17.40	70.50
	TP16-3	3.85	16.00	118.00
2021	TD66-1	0.15	4.12	15.20
	TD66-2	0.18	5.89	23.10
	TD66-3	0.06	2.56	12.60
	TE41-1	0.47	7.52	126.00
	TE41-2	0.25	5.28	16.50
	TE41-3	0.19	4.98	16.00
	TP21-1	5.33	16.60	74.10
	TP21-2	4.68	14.60	59.40
Average			**10.09**	

Table 2.3 Total suspended solids (TSS) concentration ($mg.l^{-1}$) of samples from the discharge. Analysis was carried out using pre-dried and pre-weighed filters and corrected using a blank. Data provided by Taharoa IronSands Ltd.

	TSS ($mg.l^{-1}$)
Sample 1	1239
Sample 2	1058
Sample 3	950
Average	**1082**

2.2.4 Simulations and processing

The fate and dispersal of the sediment in suspension during the discharge operation were modelled using the Delft3D hydrodynamic model coupled with waves and the sediment transport module. The modelling included a sediment fraction representative of the fine material typically present in the discharge water.

Simulations were for two distinct periods (winter and summer months) to include a range of hydrodynamic and wave conditions. The simulations covered 3 months each period. Based on the total volume of release per year (7,500,000 m^3), it is assumed a load is released approximately every 6 days during the 3 month-period, totalling 12.5 discharges (1,875,000 m^3) per 3-month period. Each discharge operation in the model assumes 48 h to completion, i.e., 75,000 m^3 per day, and a total of 150,000 m^3 per discharge event (a rate of 0.8681 $m^3.s^{-1}$).

We used a concentration of 1 $kg.m^{-3}$ as the initial concentration of sediments in the model simulations based on the TSS from laboratory analysis of samples taken from the ship loading water. To reduce computer simulation time, salinity was not included in the model. The surface plume close to the vessel may be slightly underestimated as the buoyancy effect of the freshwater discharge into the saline environment is not considered. However, as the mooring is situated in a very dynamic area, the freshwater plume is likely to mix quickly as a result of vertical mixing due to wave and currents.

According to information provided by Taharoa IronSands Ltd the depth of discharge starts at 4.48 m and increases to 13.93 m below the water surface at departure. The depth increase is a result of the ship taking on the load of ironsand. Therefore, as simulations were carried out in 3D, discharge was placed at the layer 3 of the model for the first half of the discharge time (24 h) and at layer 4 for the second half of the discharge time.

Results were processed in terms of maps of plume sediment concentration and sedimentation. The 50^{th} and 90^{th} percentile sediment concentrations were presented (concentrations that occur 50% and 10% of the simulation time). Timeseries at selected locations were also extracted.

Table 2.4 Assumptions of discharge adopted in the simulations.

simulation period	3 months	summer and winter
Total loads/period	12.5	
time discharge/load	48 h	
volume discharged/load	150,000 m^3	75,000 $m^3.day^{-1}$
discharge rate	0.8681 $m^3.s^{-1}$	
concentration	1 kg. m^3	
total rate/discharge	0.8681 kg. s^{-1}	

3. Results

3.1 Model validation

The model was validated against available wave data from the Taharoa Triaxys buoy and hindcast sea surface height (SSH) from ROMS model results. Validation site's locations are in Table 3.1. Both buoy and water levels sites are located approximately at the ship loading site. Note that all model forcings and results are in GMT+000 time. The period for validation was from 20 November 2016 to 25 December 2016.

Comparison of the modelled significant wave height (Hs) and peak period (Tp) against the buoy measurements shows a good agreement between the two datasets (Figure 3.1). The model slightly overestimates wave height and shows higher percentages of occurrence of waves from WSW, while waves from the west are underrepresented, noting that waves coming from this direction are comparatively less frequent (Figure 3.2). Peak period is slightly underestimated by the model.

Water level Delft3D model results show good agreement between sea surface height extracted from ROMS output at the ship loading site (Figure 3.3).

Table 3.1 Sites and variables for model calibration of waves and water levels.

Value	Lon; Lat	Variables
Taharoa Triaxys buoy	174.667; -38.200	Hs, Tp, Dpm
ROMS	174.667; -38.200	SSH/Water level

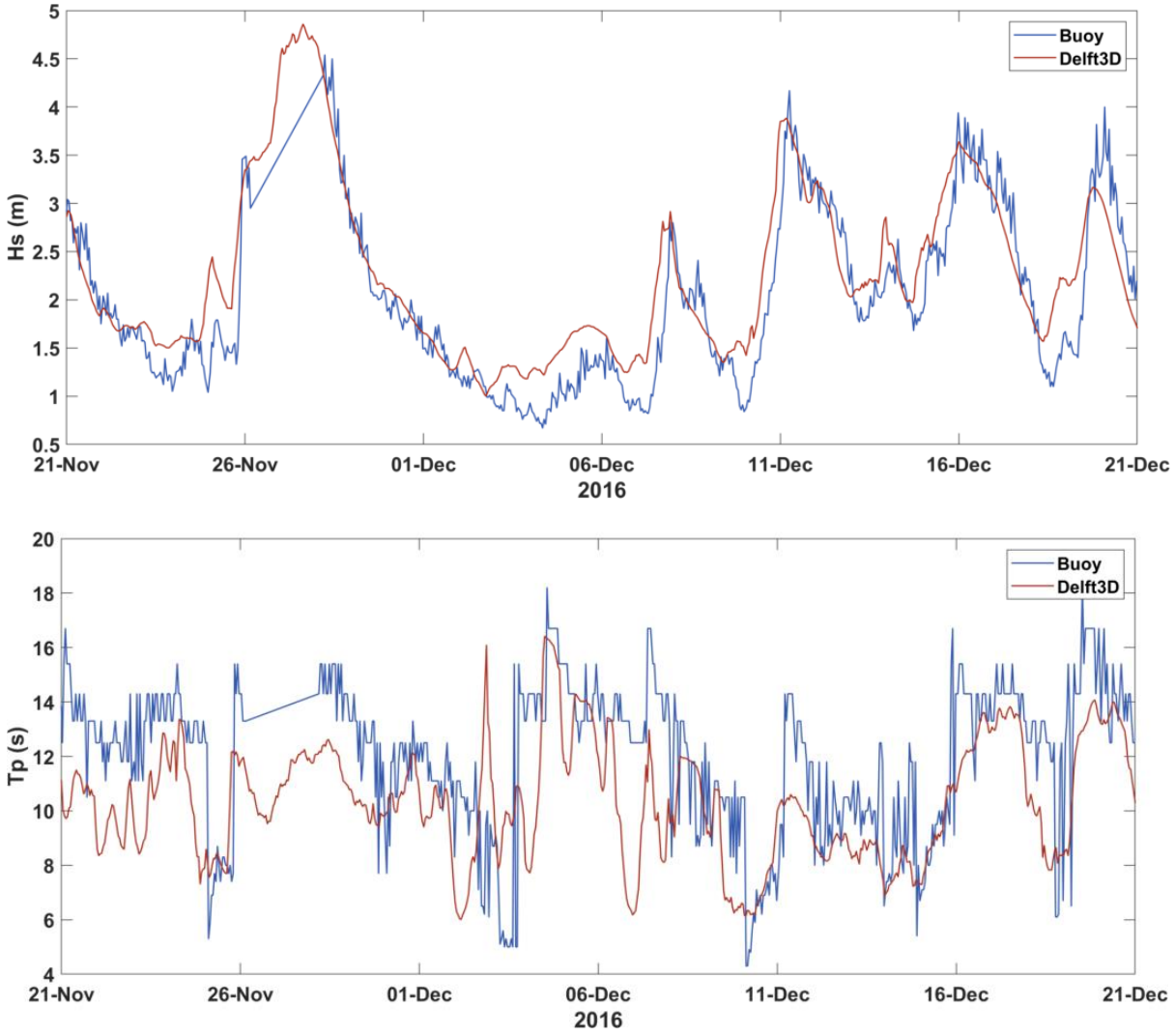

Figure 3.1 Top: Modelled significant wave height (Hs, in red) against wave buoy measured data (n blue); Bottom panel: Modelled peak period (Tp, in red) against wave buoy measured data (in blue).

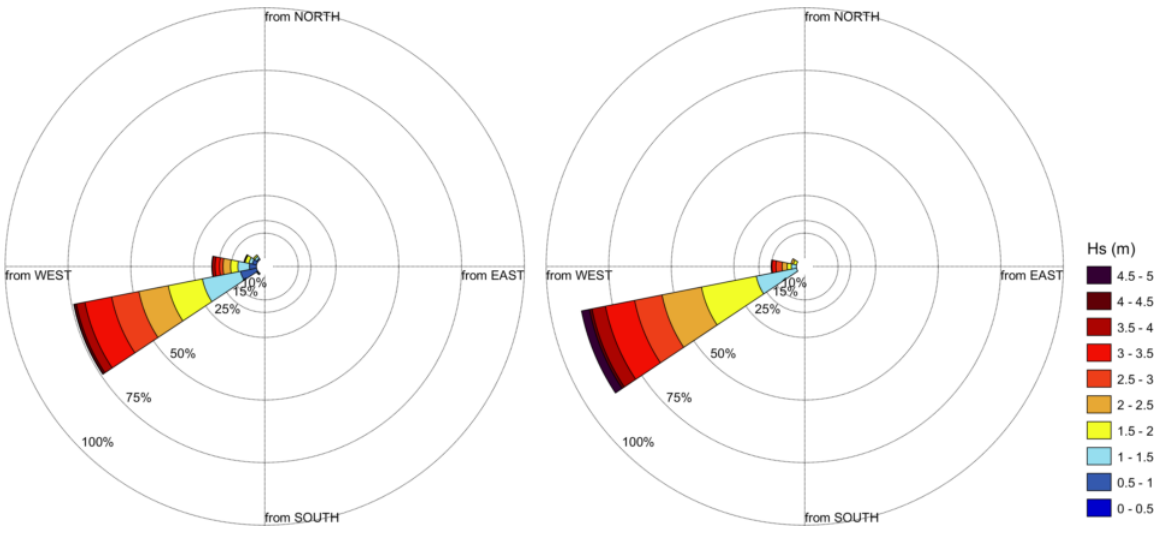

Figure 3.2 Taharoa buoy wave data (left) and Delft3D wave model results (right).

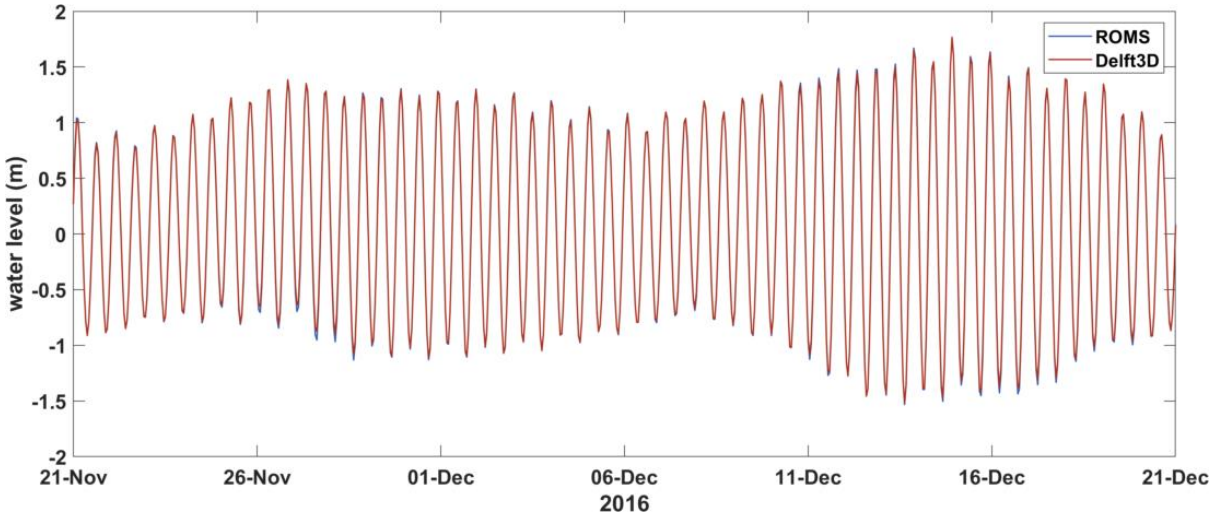

Figure 3.3 Sea surface height from ROMS (blue) at the loading site compared against Delft3D water level model results (red).

3.2 Sediment dispersion – Summer

The 50th percentile sediment concentration at surface and bottom are shown in Figure 3.4. These maps show the concentration levels **above background** that are exceeded 50% of the time. Maps of the 90th percentile (Figure 3.5) show largest concentration levels, that are exceeded only 10% of the time.

In general, higher sediment concentration is restricted to the source area and during discharge, with sediment plume dispersing along the coast to the south and to the north of the ship loading site. Sediment transport pattern tend to be mostly oriented northward.

The 50th percentile results show that concentrations are below 0.09 mg.l^{-1} (Figure 3.4). The 50th percentile (median value), means that 50% of the data are above and 50% are below it. The plume shows larger footprint in the 90th percentile maps as expected (Figure 3.5), occurring mostly along the coast, south and north of the source, with maximum concentration of 0.62 mg.l^{-1} at the surface and 0.39 mg.l^{-1} at seabed (Figure 3.5). The 90th percentile means that 90% of the values are lower than it and only 10% are above it.

The 90th percentile maps show plumes of less than 0.04 mg.l^{-1} around the area east of the Albatross Point and at the Aotea and Kawhia harbour entrances.

Snapshots of sediment plume for the first discharge event of the summer simulation (01-02 January) is presented in in Figure 3.6. Concentration is higher during the 2 days of discharge, which is quickly dissipated once the discharge operation finishes (snapshots

of the 3rd day and afterwards). The quick reduction in concentration also occurs through the water column, as shown in the profiles in Figure 3.7. Higher sediment concentrations occur at the depths of discharge for the first 2 days while concentration is significantly reduced after discharge finishes. As the simulation progresses, the profiles show slightly higher concentrations at the bottom as a result of sediment settling.

Timeseries of sediment concentration at the surface and bottom layers (Figure 3.9) are presented for 4 selected sites (shown on the map in Figure 3.8). Site 1 (loading site) shows higher concentrations during the discharge events and at the surface, which is quickly reduced once the discharge operation finishes. Concentration at the bottom layer increases as sediment settles towards seabed. Note that the range of concentration shown in the y-axis of site 1 graph is higher (0-2 $mg.l^{-1}$) than for the other sites (0-0.5 $mg.l^{-1}$).

Results at the other sites (site 2 to 4) show that low concentration (<0.5 $mg.l^{-1}$ at site 2 and <0.15 $mg.l^{-1}$ at sites 3 and 4) occurs during the simulation period, with two periods of increased concentration followed by a reduction after the last discharge event. Concentrations tend to be higher at the bottom and be more variable at these sites.

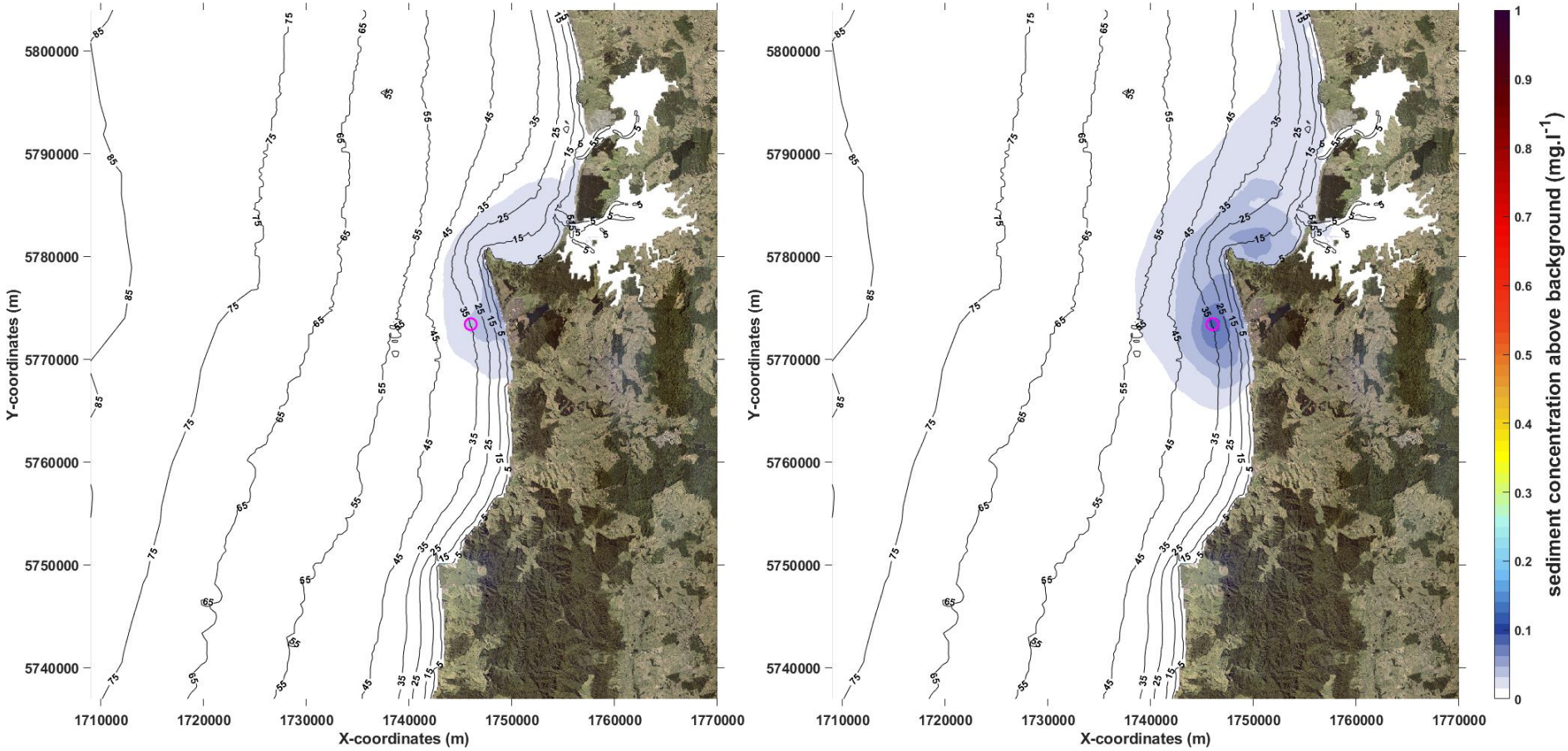

*Figure 3.4 50th percentile map of sediment concentration (mg.l^{-1}) at surface (left) and at the bottom (right) for **summer** run.*

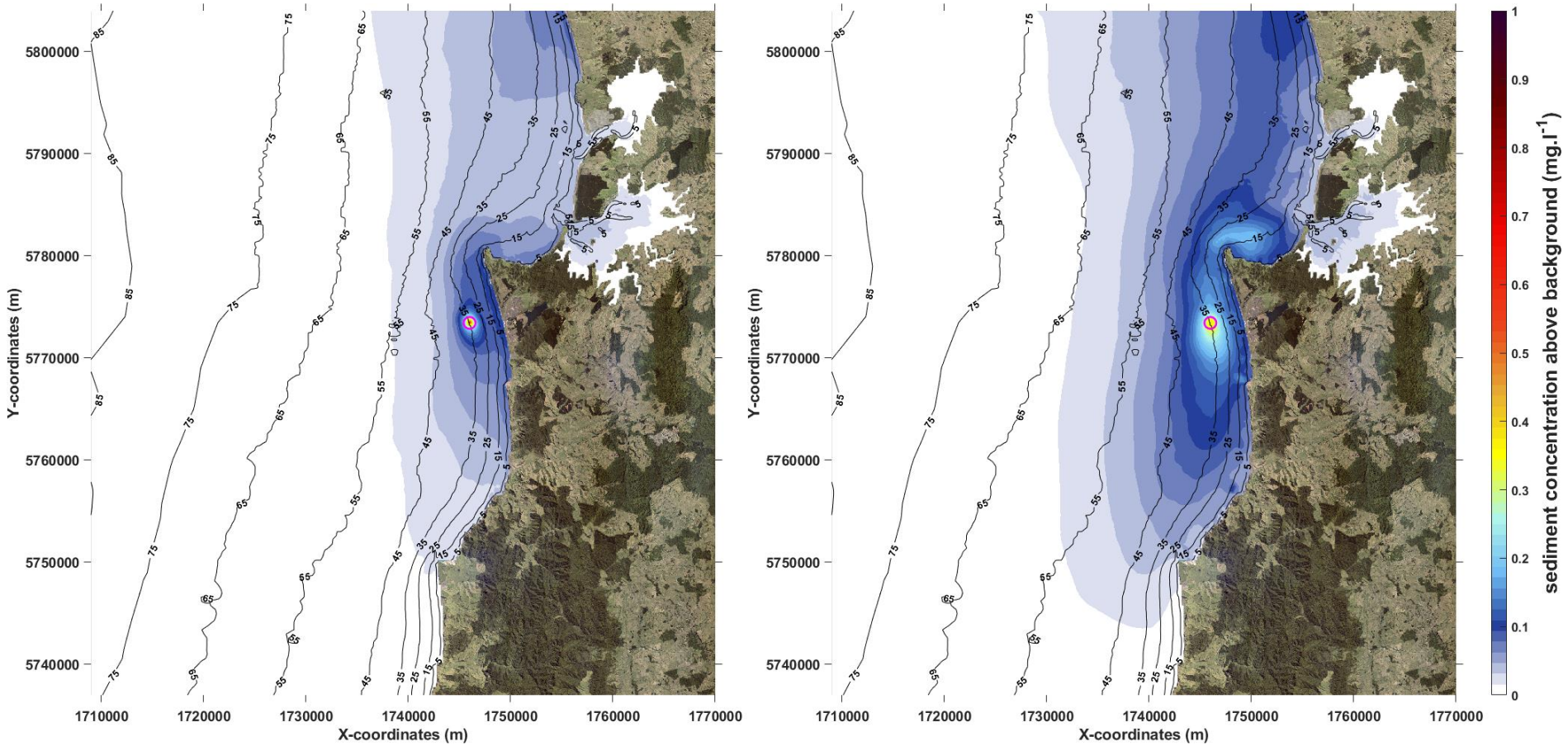

*Figure 3.5 90th percentile map of sediment concentration (mg.l-1) at surface (left) and at the bottom (right) for **summer** run.*

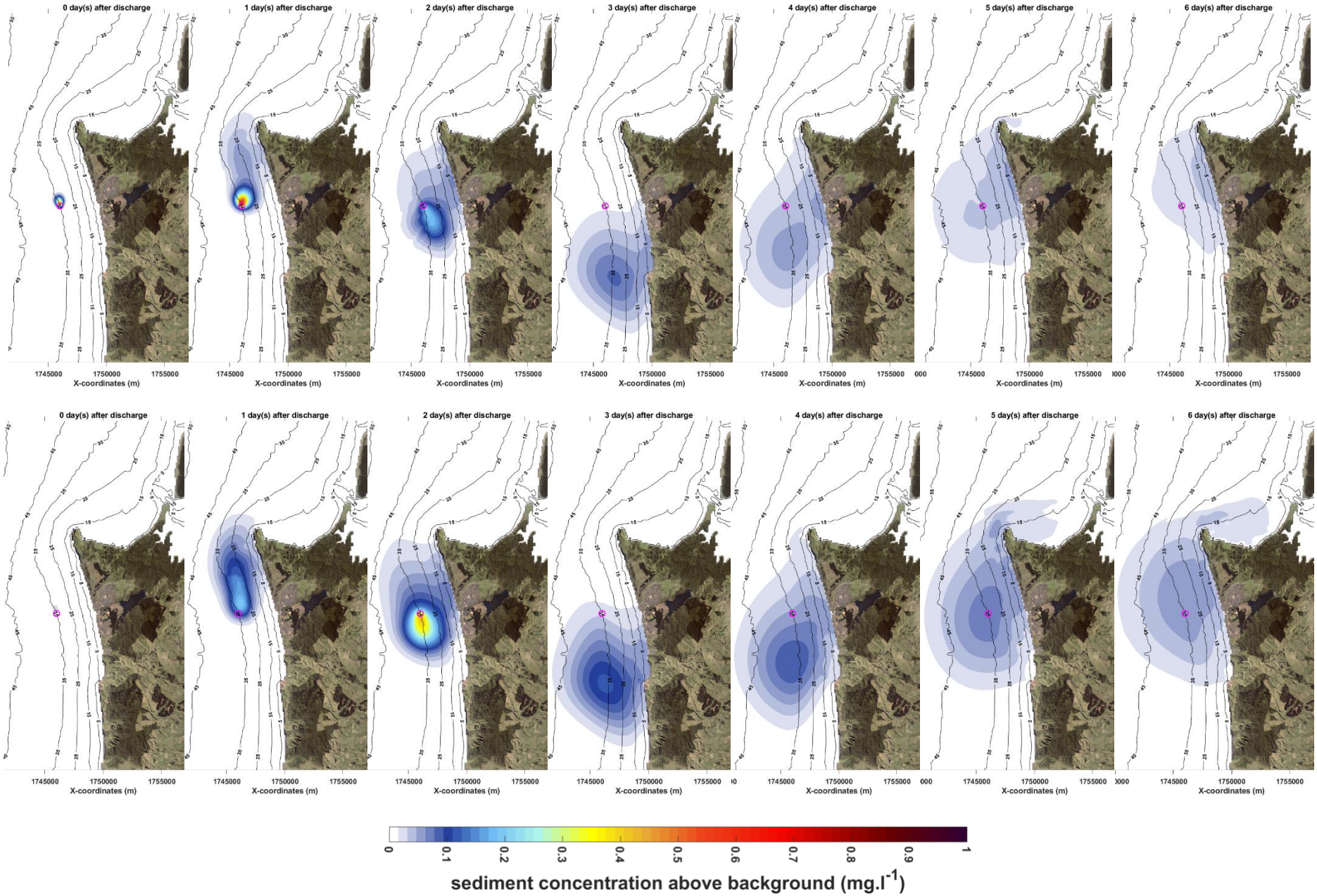

*Figure 3.6 Snapshots of plume concentration at surface (top) and bottom (bottom), 1h, and 1 to 6 days after start of first discharge for **summer** run.*

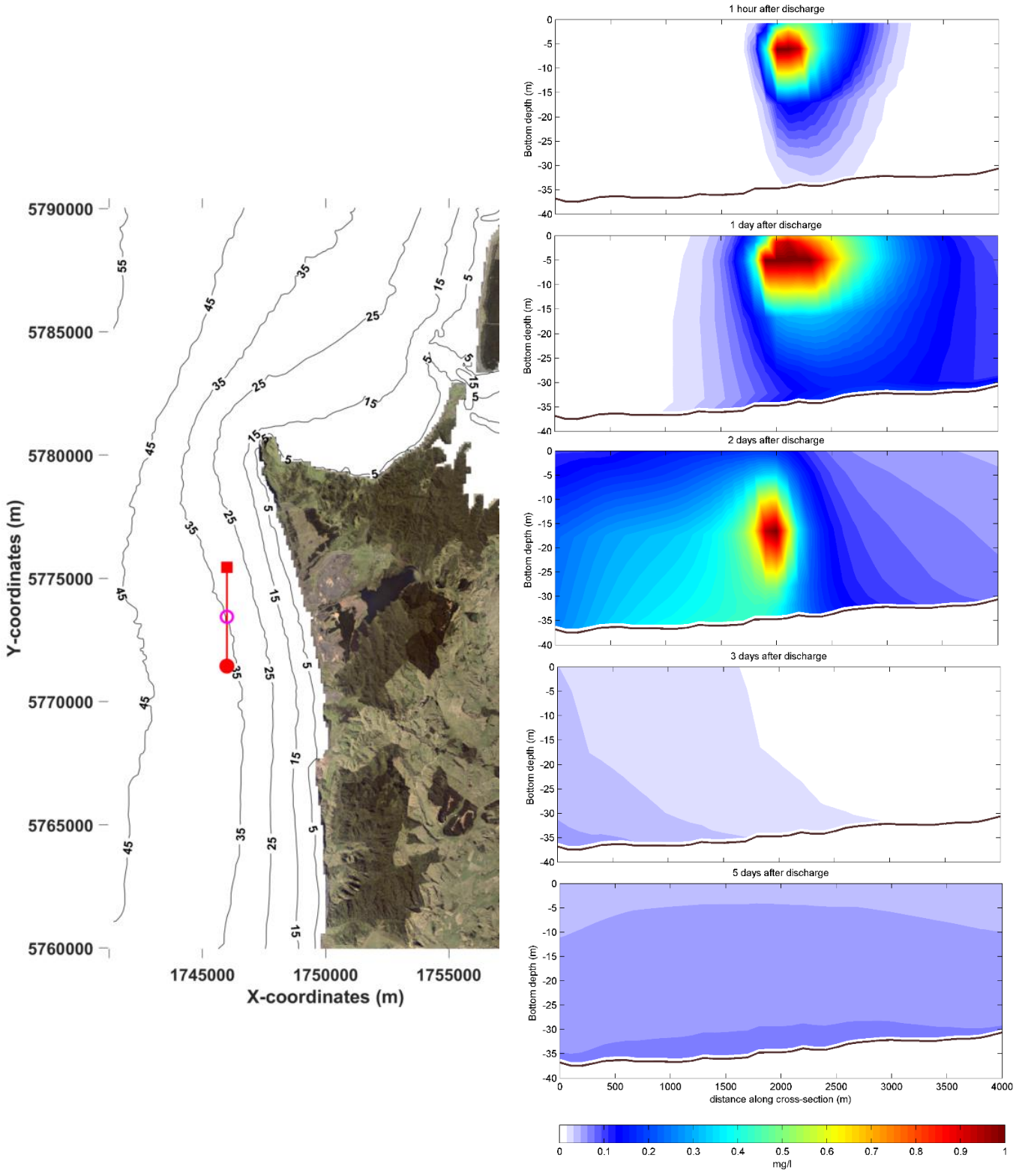

*Figure 3.7 Profiles of plume concentration 1h, 1 day, 2 days, 3 days, and 5 days after start of first discharge for the **summer** run. The circle and square on the map represent 0 m and 4000 m on the profile x-axis. The magenta circle at the centre of the profile represents the discharge location (~ 2000 m on the x-axis of profile).*

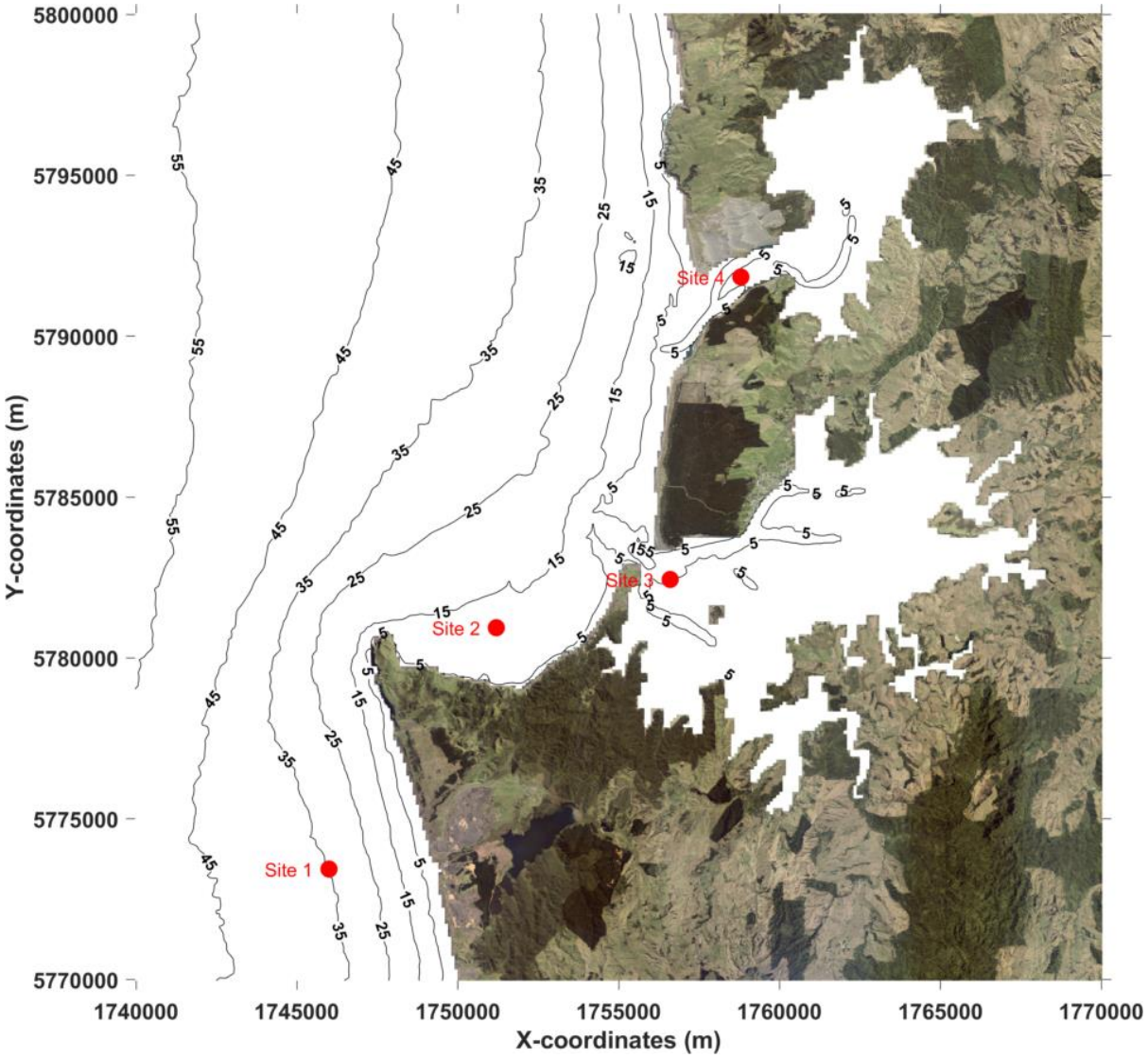

Figure 3.8 Selected sites for extraction of timeseries of model results.

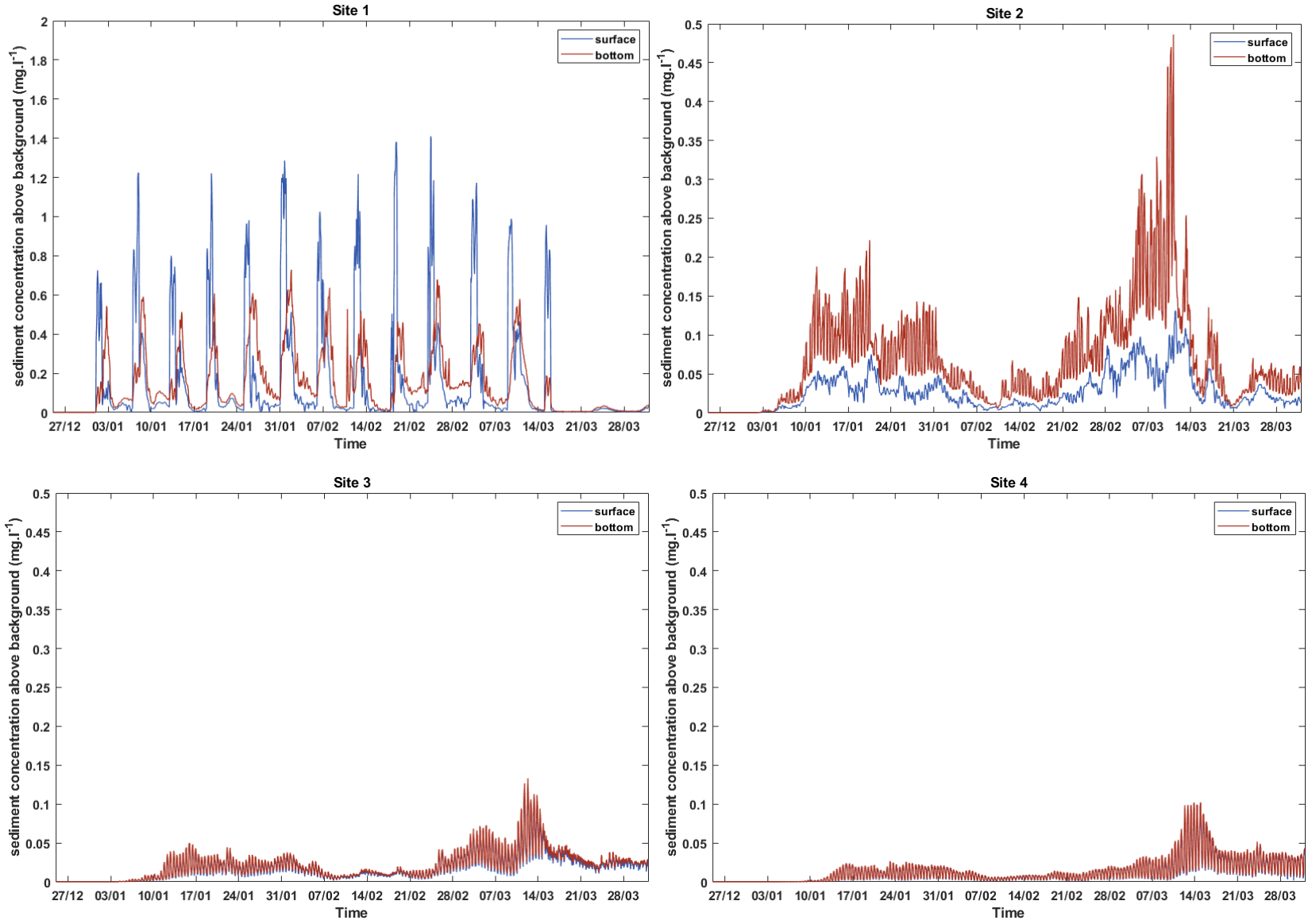

*Figure 3.9 Timeseries of sediment concentration at surface (blue) and bottom (red) layers at site 1 to site 4) for **summer** run. Note that Site 1 has different scale for better visualisation of results.*

3.3 Sediment dispersion – Winter

The 50th percentile sediment concentration at surface and bottom are shown in Figure 3.10. These maps show the concentration levels **above background** that are exceeded 50% of the time. Maps of the 90th percentile (Figure 3.11) show largest concentration levels, that are exceeded only 10% of the time.

Similar to summer, 50th percentile of plume results during winter show that higher sediment concentration is restricted to the source area. However, in winter, the plume footprint is more spread out (Figure 3.10). Concentration is slightly increased east of Albatross Point, where waves and currents wrap around the coastline, resulting in an area protected by the point from the waves coming from the SW sector. Maximum concentration that occurs 50% of the time are approximately 0.04 (surface) and 0.07 mg.l^{-1} (seabed).

The plume footprint in the 90th percentile maps for winter are more extended compared to summer runs. Maximum concentration is approximately 0.46 mg.l^{-1} at the surface and 0.31 mg.l^{-1} at seabed mainly concentrated at the sediment source and some areas around Albatross Point and north of Aotea Harbour along the coast (<0.13 mg.l^{-1}), although the increase at the north could be a result of instabilities caused by the proximity to the northern model open boundary (Figure 3.11).

Snapshots of sediment plume for the first discharge event of the winter simulation (01-02 June) is presented in in Figure 3.12. Concentration is higher during the 2 days of discharge, which is quickly dissipated once the discharge operation finishes (snapshots of the 3rd day and afterwards). Six days after the first discharge event, the plume has almost totally dissipated. The concentration through the water column is represented by the profiles in Figure 3.13. At the discharge location, concentration remains high while discharging, however, it is significantly reduced after discharge finishes.

Timeseries of sediment concentration at the surface and bottom layers (Figure 3.14) are presented for 4 selected sites (shown on the map in Figure 3.8). Concentration at loading site (site 1) is comparatively higher than the other sites (site 2-4) during the discharge events. Surface concentration is higher at the start of the discharge followed by a decrease while concentration at the bottom layer increases as sediment settles towards seabed. Note that the y-axis of site 1 graph (0-2 mg.l^{-1}) differs from the other sites (0-0.5 mg.l^{-1}). Site 2 (east of Albatross Point) shows variable peaks of increased concentrations, although concentrations remain relatively low compared to site 1 (<0.3 mg.l^{-1}) and higher concentrations at the bottom as sediment settles and disperses from the source. Site 3 and Site 4 (Kawhia and Aotea harbour entrances) show relatively lower concentrations (<0.2 mg.l^{-1}).

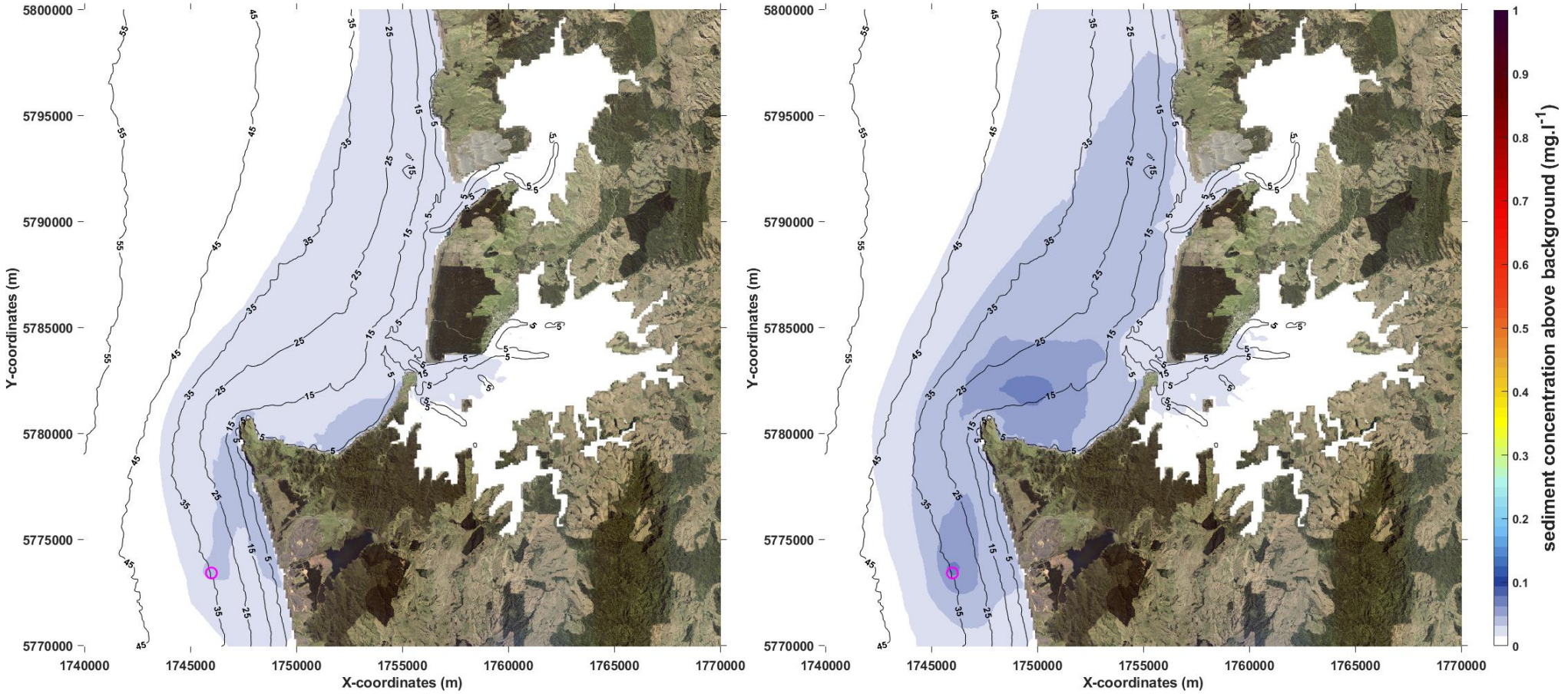

*Figure 3.10 50th percentile map of sediment concentration (mg.l^{-1}) at surface (left) and at the bottom (right) for **winter** run.*

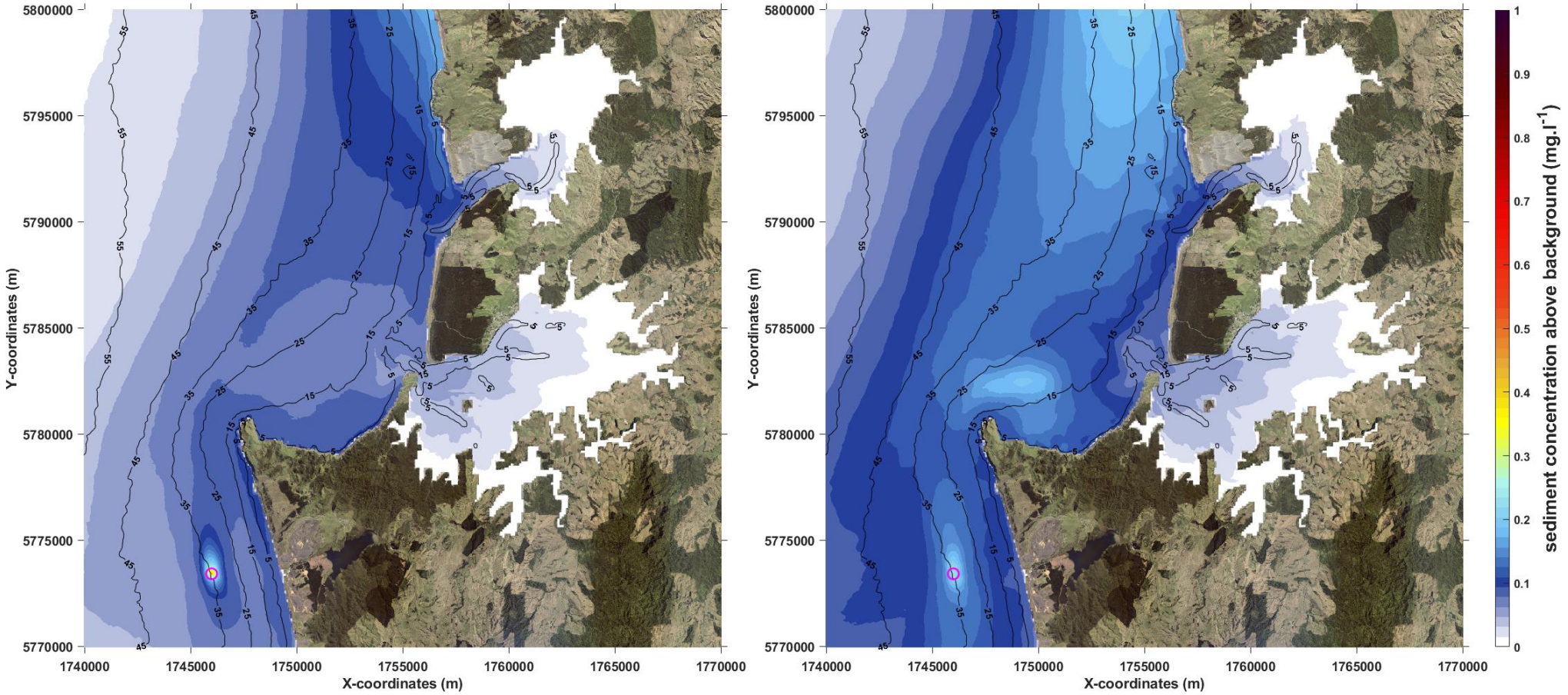

*Figure 3.11 90th percentile map of sediment concentration (mg.l-1) at surface (left) and at the bottom (right) for **winter** run.*

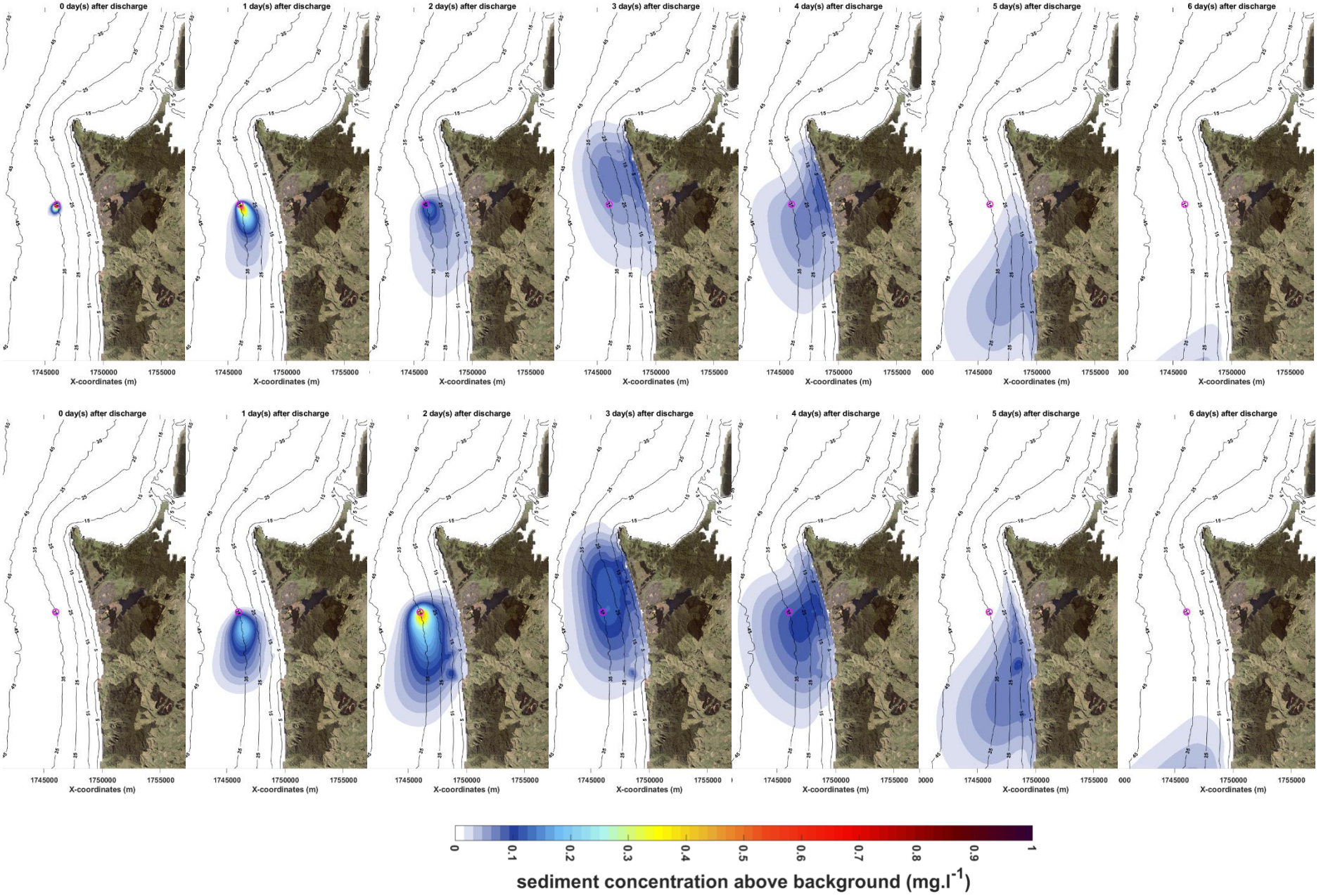

*Figure 3.12 Snapshots of plume concentration at surface (top) and bottom (bottom) 1h, and 1 to 6 days after start of first discharge for **winter** run.*

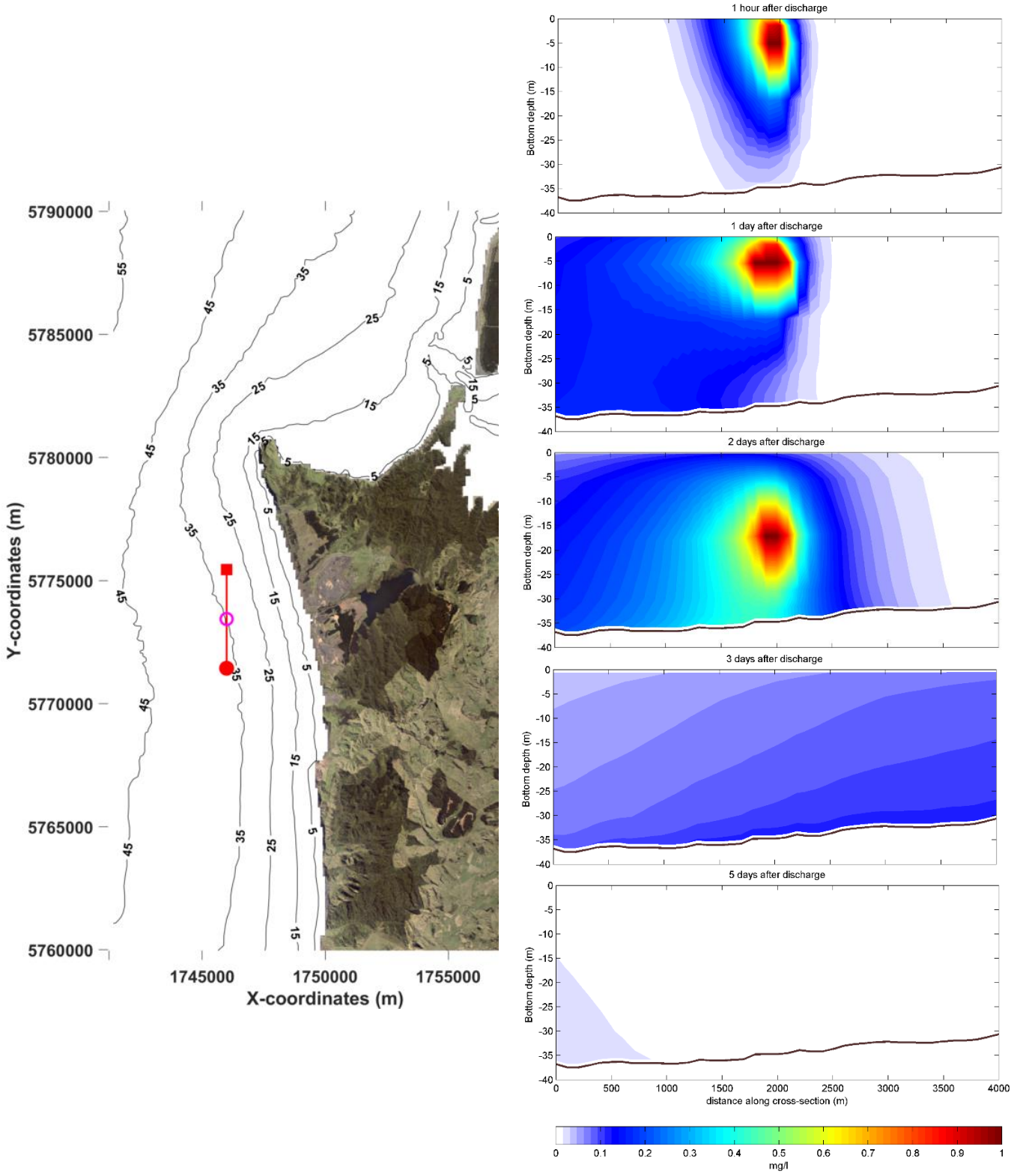

*Figure 3.13 Profiles of plume concentration 1h, 1 day, 2 days, 3 days, and 5 days after start of first discharge for **winter** run. The circle and square on the map represent 0 m and 4000 m on the profile x-axis. The magenta circle at the centre of the profile represents the discharge location (~ 2000 m on the x-axis of profile).*

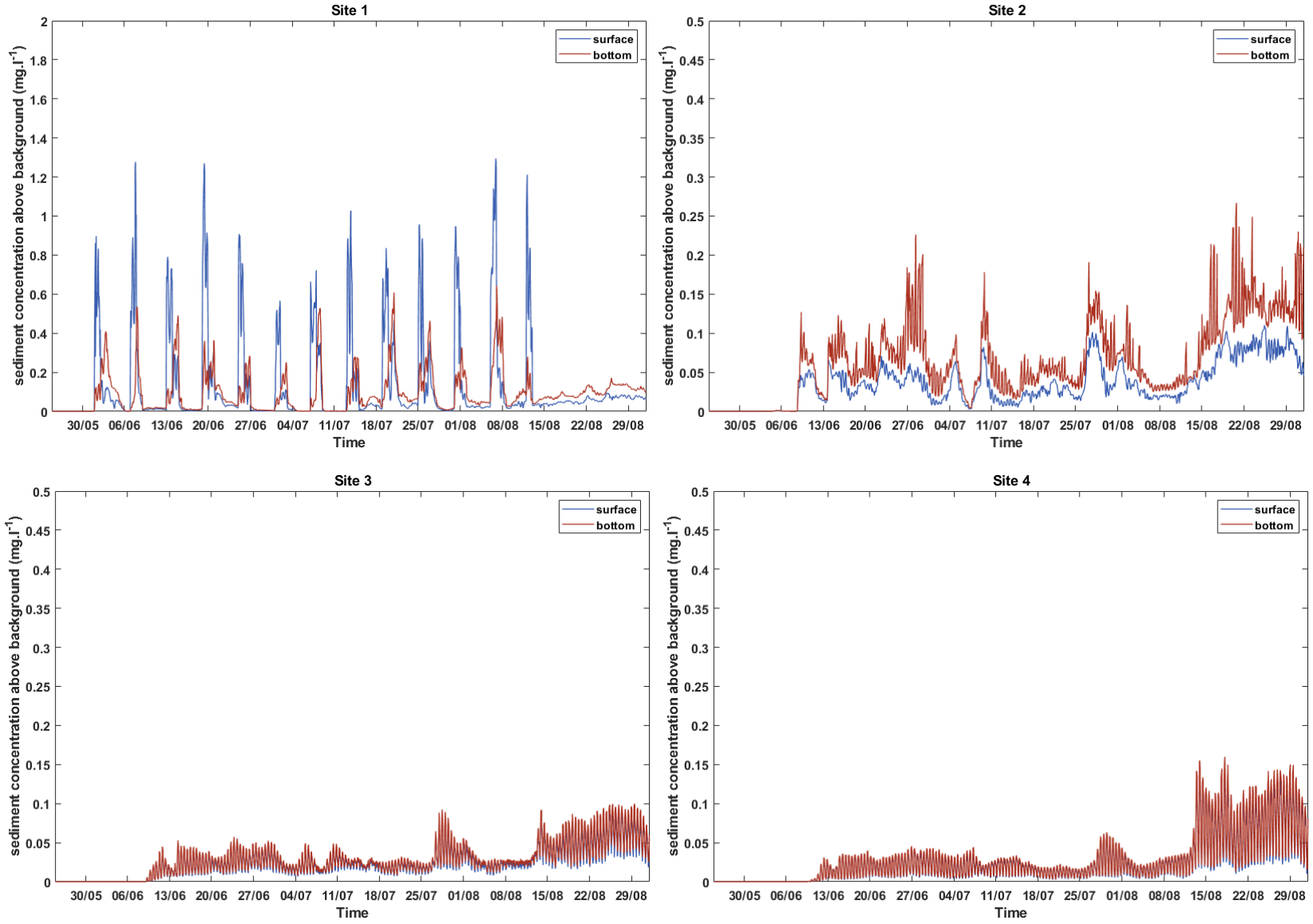

*Figure 3.14 Timeseries of sediment concentration at surface (blue) and bottom (red) layers at site 1 to site 4) for **winter** run. Note that Site 1 has different scale for better visualisation of results.*

3.4 Sediment deposition

In summer and winter, sediment deposition is particularly low (less than 0.04 mm and 0.06 mm, respectively) and occurs mostly at shallow, low energy areas within Aotea and Kawhia harbours (Figure 3.15 and Figure 3.16). As a reference, the approximate size of the sediment particle considered in the model (see Table 2.2) is of 10 µm or 0.01 mm.

To estimate the thickness of deposited sediment after one year, we calculated the final deposition as 2*(summer + winter). This result is presented in Figure 3.17. It is important to note that this calculation assumes that summer and winter are representative of the hydrodynamic conditions of a full year and of a range of variations at the study area. Results for the full year show similar depositional areas with increased thickness compared to winter and summer separately, as expected. The limits in Figure 3.17 were modified to reflect that increase and improve visualisation. The maximum deposition is approximately 0.18 mm, which remains relatively low (<1mm).

There are scattered sedimentation areas at the end of the simulation throughout the model domain (especially in deeper regions) that are of a transient nature and of no significance, being constantly modified during the simulation and does not represent a longer-term trend in deposition. These areas were removed from the plots for clarity.

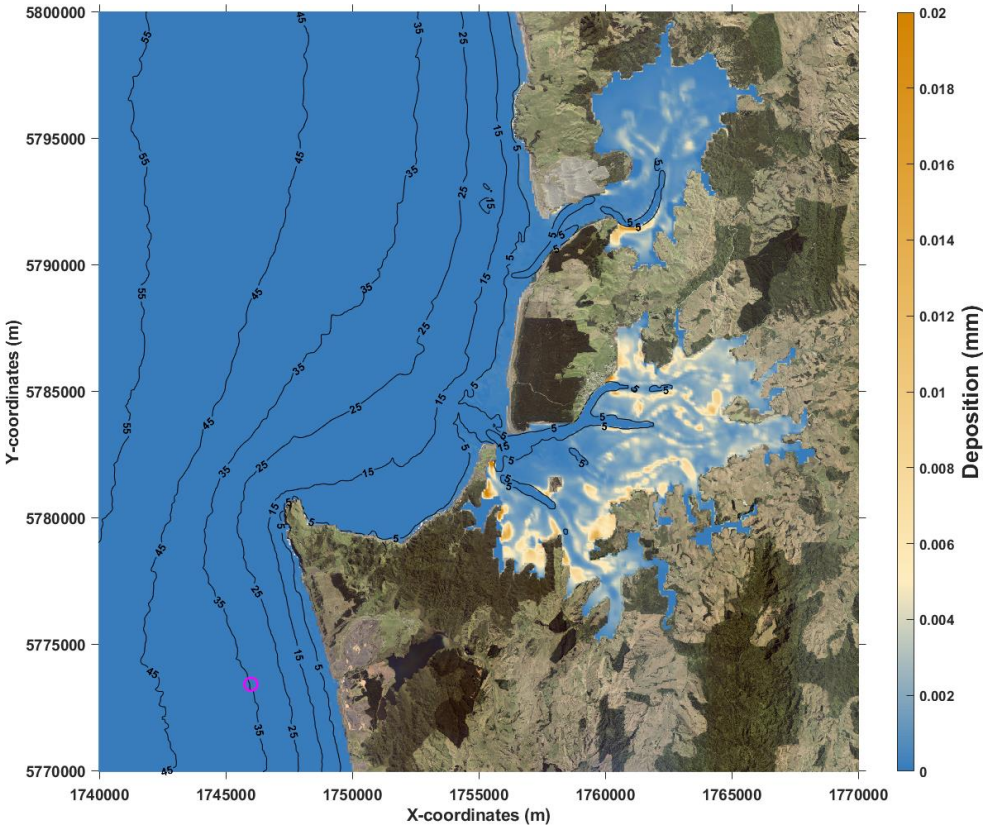

*Figure 3.15 Deposition (mm) at the end of 3-month simulation for **summer** run. The magenta circle represents the discharge location.*

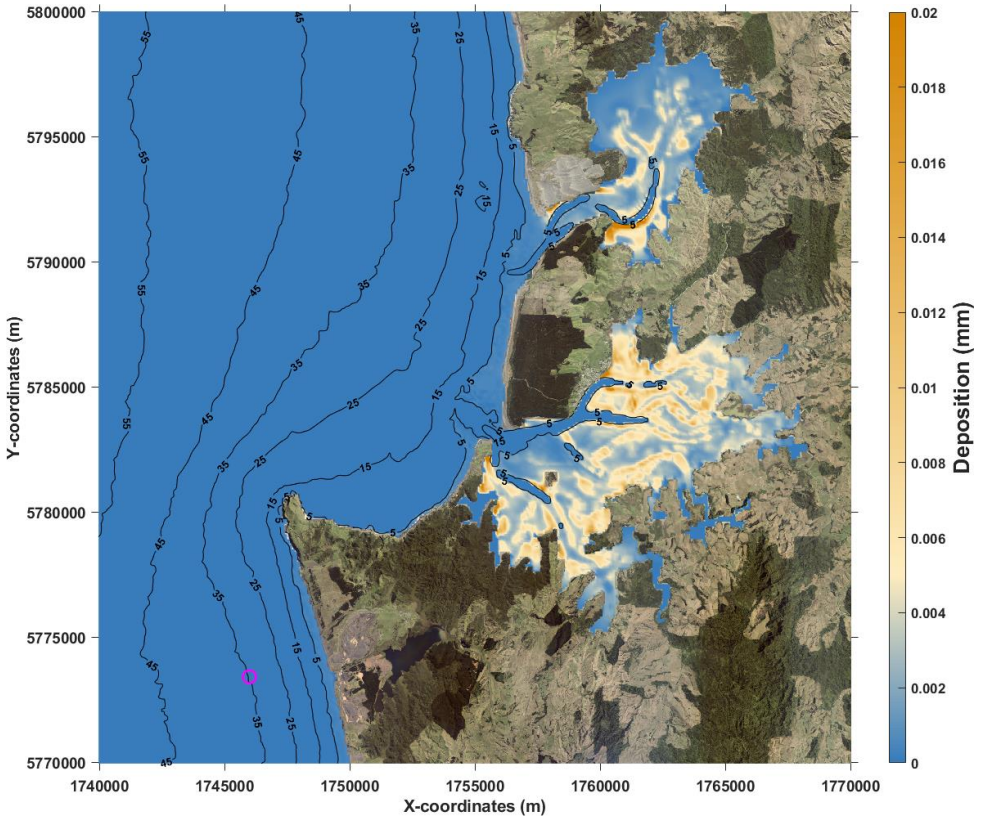

*Figure 3.16 Deposition (mm) at the end of 3-month simulation for **winter** run. The magenta circle represents the discharge location.*

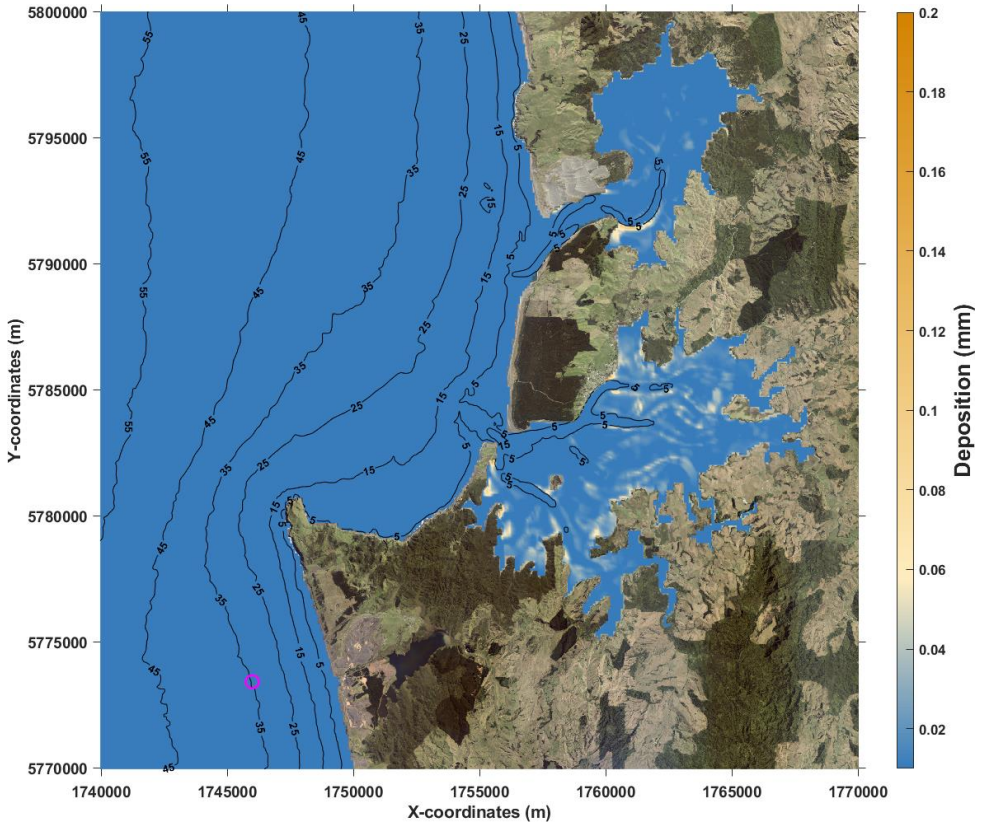

*Figure 3.17 **Yearly** deposition (mm) combining the summer and winter runs, calculated as 2*(summer+winter). The magenta circle represents the discharge location.*

4.Summary

Taharoa Ironsands Limited has applied to continue to undertake iron sand mining operations near Taharoa. The extracted iron sand is loaded into ships and de-watering occurs during loading operations. MetOcean Solutions has previously undertaken a plume dispersion and deposition modelling (MetOcean Solutions, 2022) which was based on the release of a total 3,600,000 m^3 of de-watering fluid per year. Taharoa Ironsands has requested that the modelling is updated to simulate the total de-watering volume proposed to be discharged each year (7,500,000 m^3), as opposed to a representative sample.

A comprehensive consideration of coastal process is required which includes an assessment of plume dynamics and dispersal (duration/extent), settling conditions, weather events and the other effects that may persist and propagate resuspension of discharged material. For this purpose, we used a calibrated and validated Delft3D model to simulate scenarios of sediment release representing the discharge of water during ship loading for two contrasting periods (summer and winter).

Results show that in general, higher sediment concentration is restricted to the source area and lower concentrations occur as it disperses along the coast. Sediment transport pattern is mostly north-south oriented.

Snapshots of the sediment plume during and after a discharge event and timeseries of sediment concentration show that areas of higher concentration (at the discharge source) are quickly dissipated once the discharge operation finishes. Higher sediment concentrations occur at the depths of discharge for the first 2 days and is significantly reduced after discharge finishes.

At areas of high sediment concentration, levels are below 0.09 $mg.l^{-1}$ for 50% of the simulation. The 90^{th} percentile results show maximum concentration of approximately 0.62 $mg.l^{-1}$ at the surface and 0.39 $mg.l^{-1}$ at the bottom. Some sediment is likely to be transported to Aotea and Kawhia harbours entrances, with maximum concentration <0.13 $mg.l^{-1}$.

The concentration of sediment released in the simulations was an average TSS value from samples taken from the ship loading water. Based on the maximum and minimum concentrations of these samples (see Table 2.3), results presented here could range from 0.9 to 1.2 times the values displayed on the figures.

Sediment deposition at the end of the 3-month runs (<0.04 and <0.06 mm for summer and winter, respectively) and for a calculated yearly deposition (<0.2 mm) is considered very low and occurs mostly within Aotea and Kawhia harbours at very low energy areas.

5.References

Ardhuin, F., Rogers,E., Babanin, A. V., Filipot, J. F., Magne, R., Roland, A., Van Der Westhuysen, A., Queffeulou, P., Lefevre, J. M., Aouf, L., & Collard, F. (2010). Semiempirical dissipation source functions for ocean waves. Part I: Definition, calibration, and validation. *Journal of Physical Oceanography*, *40*(9), 1917–1941.

Booij, N., Ris, R. C., & Holthuijsen, L. H. (1999). A third-generation wave model for coastal regions: 1. Model description and validation. *Journal of Geophysical Research: Oceans*, *104*(C4), 7649–7666.

Carter, L., & Heath, R. A. (1975). Role of mean circulation, tides, and waves in the transport of bottom sediment on the New Zealand continental shelf. *New Zealand Journal of Marine and Freshwater Research*, *9*(4), 423–448.

Collins, J. (1972). Prediction of Shallow Water Spectra. *Journal of Geophysical Research*, *77*(15), 2693–2707.

Deltares. (2013). *User Manual Delft3D-FLOW. version: 3.15.2789*. Deltares. http://oss.deltares.nl/web/delft3d/manuals

Deltares. (2018). *User Manual Delft3D-FLOW* (Version: 3.15). Deltares.

Egbert, G. D., & Erofeeva, S. Y. (2002). Efficient inverse modelling of barotropic ocean tides. *Journal of Atmospheric and Oceanic Technology*, *19*(2), 183–204.

Ferry, N., Parent, L., Garric, G., Bricaud, C., Testut, C. E., Le Galloudec, O., Lellouche, J. M., Drevillon, M., Greiner, E., & Barnier, B. (2012). GLORYS2V1 global ocean reanalysis of the altimetric era (1992–2009) at meso scale. *Mercator Ocean–Quarterly Newsletter*, *44*.

Fredsøe, J. (1984). Turbulent Boundary Layer in Wave-current interaction. *Journal of Hydraulic Engineering, ASCE*, *110*, 1103–1120.

Hersbach, H., Bell, B., Berrisford, P., Biavati, G., Horányi, A., Muñoz Sabater, J., Nicolas, J., Peubey, C., Radu, R., Rozum, I., Schepers, D., Simmons, A., Soci, C., Dee, D., & Thépaut, J.-N. (2018). *ERA5 hourly data on single levels from 1979 to present*. Copernicus Climate Change Service (C3S) Climate Data Store (CDS).

Hicks, D. M., Shankar, U., McKerchar, A. I., Basher, L., Jessen, M., Lynn, I., & Page, M. (2011). Suspended sediment yields from New Zealand rivers. *Journal of Hydrology (NZ)*, *50*(1), 81–142.

Hunt, S., & Jones, H. F. E. (2020). The fate of river-borne contaminants in the marine environment: Characterising Regions of Freshwater Influence (ROFIs) and estuary plumes using idealised models and satellite images. *Marine Pollution Bulletin*, *156*, 111169.

MacDonald, I., Budd, R., Bremner, D., & Edhouse, S. (2012). *South Taranaki Bight Iron Sand Mining: Oceanographic measurements data report* (Nos. HAM2012-147). NIWA.

MetOcean Solutions. (2022). *Discharge Dispersion Modelling. Iron Sand Mining Operations—Taharoa* (No. Report P0564 v1.0).

Ramli, A. Y., de Lange, W., Bryan, K., & Mullarney, J. (2015). *Coupled flow-wave numerical model in assessing the impact of dredging on the morphology of Matakana Banks*. 758.

Ris, R. C., Holthuijsen, L. H., & Booij, N. (1999). A third-generation wave model for coastal regions: 2. Verification. *Journal of Geophysical Research: Oceans*, *104*, 7667–7681.

Saha, S., Moorthi, S., Pan, H.-L., Wu, X., Wang, J., Nadiga, S., Tripp, P., Kistler, R., Woollen, J., Behringer, D., Liu, H., Stokes, D., Grumbine, R., Gayno, G., Wang, J., Hou, Y.-T., Chuang, H.-Y., Juang, H.-M. H., Sela, J., … Goldberg, M. (2010). The NCEP Climate Forecast System Reanalysis. *Bulletin of the American Meteorological Society*, *91*(8), 1015–1057. https://doi.org/10.1175/2010BAMS3001.1

Tolman, H. L. (1991). A Third-Generation Model for Wind Waves on Slowly Varying, Unsteady, and Inhomogeneous Depths and Currents. *Journal of Physical Oceanography*, *21*(6), 782–797. https://doi.org/10.1175/1520-0485(1991)021<0782:ATGMFW>2.0.CO;2

Weppe, S., McComb, P., & Coe, L. (2015). Numerical model studies to support the sustainable management of dredge spoil deposition in a complex nearshore environment. In *Coastal Sediments 2015* (Vol. 1–0). World Scientific. http://www.worldscientific.com/doi/abs/10.1142/9789814689977_0113

Williams, R. D., Measures, R., Hicks, D. M., & Brasington, J. (2016). Assessment of a numerical model to reproduce event-scale erosion and deposition distributions in a braided river. *Water Resources Research*, *52*, 6621–6642.